AI-AEC-13088

ZIRCONIUM HYDRIDE REACTOR CORE HEAT TRANSFER STUDIES SUMMARY REPORT

AEC Research and Development Report

Atomics International Division
Rockwell International

P.O. Box 309
Canoga Park, California 91304

DISCLAIMER

NOTICE

Printed in the United States of America
Available from
National Technical Information Service
U.S. Department of Commerce
5285 Port Royal Road
Springfield, Virginia 22151
Price: Printed Copy $3.00; Microfiche $0.95

AI-AEC-13088
SNAP REACTOR
SNAP PROGRAM
M-3679-R69
C-92b

ZIRCONIUM HYDRIDE REACTOR CORE HEAT TRANSFER STUDIES SUMMARY REPORT

A. R. MARCHESE
A. N. GALLEGOS

Atomics International Division
Rockwell International

P.O. Box 309
Canoga Park, California 91304

CONTRACT: AT(04-3)-701
ISSUED: JUNE 15, 1973

DISTRIBUTION

This report has been distributed according to the category "Systems for Nuclear Auxiliary Power (SNAP) Reactor – SNAP Program," as given in the Standard Distribution for Classified Scientific and Technical Reports, M-3679.

CONTENTS

TABLES

FIGURES

FIGURES

FIGURES

ABSTRACT

This report presents the results of an experimental study showing the influence of rod spacers on the heat transfer to a liquid metal (NaK-78) in turbulent longitudinal flow through a closely spaced rod bundle. The rod bundle consisted of 19 electrically heated elements, which were arranged on hexagonal arrays having a pitch-to-diameter (P/D) ratio of 1.05. Two rod configurations, each with a different type of rod spacer, were investigated. The first configuration utilized ring spacers which were banded to the outer surface of each test rod. For the second configuration, helical-fin spacers were attached to the cladding tubes. Besides maintaining uniform rod spacing, the purpose of the rod spacers was to promote increased fluid turbulence and mixing.

Heat transfer results for the cladding circumferential temperature distribution and the rod-average film coefficients were obtained over a range of heating and flow conditions of interest to compact reactor cores. For the rod-average film coefficient, the helical fin configuration showed a significant improvement over the predicted smooth tube results. In the flow range investigated, the heat transfer results were found to be essentially independent of the coolant Peclet number.

BLANK

I. INTRODUCTION

A series of compact nuclear reactors and electrical power systems were designed, developed, and tested for the Space Nuclear Auxiliary Power (SNAP) Program. The zirconium hydride reactors for these systems were fueled by hydrided zirconium-uranium elements enclosed within high-temperature, corrosion-resistant tubes. Windows in the external beryllium neutron reflector were adjusted by rotating the drums or sliding the segments to regulate the neutron loss from the core, and thus the power output of the reactor. The direct-radiating, thermoelectric-module-powered Power Conversion System (PCS) produced over 500 w of electrical power on the flight-tested SNAP 10A system. Mercury-Rankine cycle turbogenerator PCS of 3- and 30-kwe power range were demonstrated for the SNAP 2 and SNAP 8 systems respectively. The latest 5-kwe Thermoelectric System was based on the compact tubular thermoelectric PCS. The NaK, used to transfer the heat from the reactor to the PCS and then from the PCS to the space radiator, was circulated by dc conduction-type electromagnetic pumps on the thermoelectric systems and by mechanical centrifugal pumps on the Mercury-Rankine systems.

Liquid metal NaK coolant is circulated through the spaces between the fuel elements within the core vessel to transfer the nuclearly generated heat to the PCS. The characteristics of the heat transfer between the fuel element and the flowing NaK coolant influences the design and the performance of the compact ZrH reactor. Series of analytical and experimental studies have been conducted to provide information useful for the design and performance evaluation of typical SNAP reactors. The results of these studies, previously reported,[1-3] are summarized in this report.

A. NEED FOR THE EXPERIMENTAL STUDIES

As the pitch-to-diameter (P/D) ratio of fuel rods in a nuclear reactor is reduced, the rod-average heat transfer coefficient is decreased, and the rod circumferential temperature gradient is increased. For closely packed ($P/D \leq 1.05$) rod bundles cooled by liquid metals, azimuthal temperature variations can be large enough to create severe thermal stress, corrosion, and hot-spot problems. In addition, rod bundles which have no intermediate tube-spacing

devices along their length are subject to degrading asymmetry effects. The asymmetry created by rod bowing and dimensional tolerances can increase rod circumferential temperature gradients above their symmetrical values. Dwyer[4, 5] and Hsu[6,7] studied the problem of geometrical asymmetry caused by dislocating a rod from its symmetrical position. They found that the asymmetry strongly affected the temperature field in the coolant flow area, causing deterioration in heat transfer capability of the displaced rod.

The preceding peripheral temperature variations could be minimized by designing for larger P/D ratios; however, from considerations of nuclear performance and space power applications, close rod spacings ($P/D \leq 1.05$) are desirable. Except for the case of P/D = 1.00, these low P/D rod bundles require rod spacing devices to guarantee positive tube spacing and to minimize asymmetry effects. Because of the positive tube spacing, and the fact that rod spacing devices cause added fluid turbulence and inter-channel mixing, it was expected that the rod bundle heat transfer performance would improve significantly over the case corresponding to P/D = 1.00. It was the primary objective of these investigations to determine the extent of this improvement.

Prior to the present studies, Subbotin et al., in the USSR, were the only researchers who had published experimental results for liquid metals flowing through rod bundles with the $P/D < 1.10$. For the case of P/D = 1.00 (i. e., where the rods are contacting each other), Subbotin et al.[8, 9] present heat transfer results for both Hg and NaK. Their Nusselt number (Nu) results exhibit a Peclet number (Pe) dependence which is not consistent with theoretical predictions for the flow range investigated. Since the authors did not mention the oxygen content of the liquid metals, and the steps taken to insure that the experimental loop was very clean, Dwyer[10] suggests the possibility of contaminants and poor thermal contact at the wall. This would cause the Nu results to be lower than would exist for a perfectly clean system, and explain the observed Pe dependence.

B. BASIC TEST METHOD

For the experimental study reported here, three rod bundle configurations were tested under conditions of turbulent longitudinal flow of NaK. Each rod bundle configuration consisted of the same 19 electrically heated elements, which

were arranged on symmetrical equilateral triangular arrays. The first configuration had all elements in contact, corresponding to P/D = 1.00. The second and third configurations, which were positively spaced, corresponding to P/D = 1.05, utilized rod spacing devices. Ring spacers, which were banded to the OD of each test element, were used for the second bundle configuration; and helical-fin spacers, which were brazed to the cladding tubes, were used for the third configuration. To determine the rod azimuthal temperature variation, small-diameter thermocouples were attached to the cladding tubes on all heaters. In addition, measurements were made of the test section inlet and outlet coolant temperature distributions, the power supplied to each test rod, and the coolant flow rate. From these measurements, rod-average heat transfer coefficient, and Nu variations with Pe, were determined.

The last section of this report describes the present status of a test assembly that was to be used for a final core verification heat transfer test, in support of the 5-kwe Reactor Thermoelectric Unmanned System Test.

II. THEORETICAL CONSIDERATIONS

An analytical model[1] has been developed to predict the heat transfer results for turbulent longitudinal flow of liquid metals through closely packed fuel rod bundles. The model was developed for the low turbulent Pe regime for liquid metals, where the eddy-thermal diffusivity is negligible, compared to the molecular diffusivity. The theoretical model was verified by data from experimental studies.[2] The model uses a finite-difference method to solve simultaneously the differential energy equations representing the heat transfer within the coolant stream and various fuel element regions. This is the so-called "multi-region" method of solution, and no assumptions are made regarding the constancy of temperature or heat flux at any of the boundary surfaces. Various "single-region" solutions, which consider the heat transfer within the coolant region alone, have been presented in the literature, but these become invalid for close rod spacings ($P/D \leq 1.10$).

To obtain a solution for the coolant energy balance, the model made use of empirical velocity relations of Levchenko et al,[11] obtained for turbulent longitudinal flow through a tightly packed rod bundle having a $P/D = 1.00$. Although the results presented in References 1 and 2 were for the case of contacting rods (i.e., $P/D = 1.00$), the analytical model can be used for other P/D ratios, simply by modifying the coolant flow area and using appropriate turbulent velocity relations. For the case of positive rod spacing, this was accomplished by enlarging the coolant flow nodal grid, and using the empirical velocity relations of Eifler and Nijsing,[12] obtained for turbulent flow through a rod bundle with a $P/D = 1.05$.

For P/D ratios of 1.00 and 1.05, the predicted heat transfer results for the cladding azimuthal temperature variation and the rod-average film coefficient will be presented later, and compared with results of the experimental study. It must be emphasized that the theoretical model considers only smooth tubes, and does not account for the increased fluid turbulence and mixing generated by rod spacers. However, for the case of $P/D = 1.05$, comparison between the predicted and experimental results does provide an insight into the influence of rod spacers on the heat transfer performance of rod bundles cooled by turbulent longitudinal flow of liquid metals.

III. FUEL ELEMENT AND CORE THERMAL SIMULATION

For the heat transfer experiments, primary emphasis was placed on providing a good thermal simulation of a ZrH core by using a bundle of electrically heated test rods. For rod bundle heat transfer studies at high P/D ratios, simulation of a reactor core can be provided by simply duplicating flow and heating conditions for a particular rod arrangement. The internal physical characteristics of the test rods are usually not important at high P/D ratios; however, this is not the case for P/D ratios near 1.00, where heat transfer coupling exists between the coolant stream and internal heater regions. For P/D near 1.00, thermal simulation becomes more complex, because of the dependence of the azimuthal heat transfer gradients on the thermal and dimensional characteristics of the heater element.

A typical ZrH core consists of a bundle of closely spaced ($1.00 \leq P/D \leq 1.05$) fuel rods, arranged on hexagonal arrays and cooled by a liquid metal, NaK-78. The Peclet number, which characterizes the coolant flow, extends over the range of 30 to 150. Heat fluxes up to 10^5 Btu/hr-ft^2, and coolant temperatures in the range of 1000 to 1200° F, are representative. The fuel rods consist of an alloy of zirconium and uranium, which is massively hydrided. The fuel rods are clad in thin-wall tubing — Hastelloy X and Inconel 800 tubing with wall thicknesses in the range of 0.010 to 0.030 in. The cladding tubing is coated internally with a 2-mil thick ceramic barrier to inhibit hydrogen moderator leakage. To accommodate fuel rod swelling and thermal expansion, a 3 to 6 mil radial hydrogen gas gap exists between the fuel rod and cladding tube. Typical values for the outer diameter and active length of the fuel element are 9/16 and 17 in. respectively.

For P/D near 1.00, all regions of the fuel element must be accounted for in the thermal analysis. Therefore, to describe the heat transfer characteristics of a ZrH fuel element, a five-region analytical model was chosen for study.[1] The gas gap, ceramic barrier, and cladding tube were represented by Regions 1, 2, and 3, respectively. Including the fuel and coolant sections gave a total of five regions. To determine the effect on heat transfer, results were determined[1] for a range of thermal conductivities and thicknesses of the various ZrH fuel element regions. The results showed that the magnitude of the circumferential temperature and heat flux gradients, which determine the rod-average

film coefficient, are dependent upon the ratios of conductivities and thicknesses of the various fuel element regions. By increasing the thermal conductivity and thickness of a particular fuel element region, circumferential heat flow was enhanced. Improving the circumferential heat flow through a region resulted in a decreased azimuthal temperature gradient and an increased heat transfer coefficient.

A four-region ZrH fuel element (without the presence of a gas gap) was also studied.[1] Comparison of the four- and five-region results showed that the influence of a gas gap on heat transfer is appreciable. The gas gap, in effect, insulates the fuel from the cladding. This results in reduced azimuthal heat flow through the fuel region, and an increased cladding circumferential temperature variation. With the fuel in contact with the cladding, there is greater circumferential heat flow, smaller cladding peripheral temperature variation, and a greater average heat transfer coefficient. From the standpoint of thermal simulation, the existence of a hydrogen gas gap in a ZrH fuel element had an important influence on the selection of a suitable test rod.

To closely simulate the thermal behavior of a ZrH fuel element with an electrically heated test element, the azimuthal variations of temperature and heat flux must be closely matched, under identical coolant flow, heating, and geometrical conditions. To reproduce the peripheral heat transfer gradients, the thermal conductivities and thicknesses of the different regions of the heater element must bear a certain relationship to one another. A typical heater element consists of an electric coil surrounded by a suitable electrical insulator and clad in a metal tube. The heat transfer characteristics of such a heater element in a tightly packed array can be described by a three-region fuel element model.[1] Thus, a heater element design can be determined which closely simulates a five-region ZrH fuel element. This is accomplished by comparing the azimuthal temperature and heat flux gradients until a close match is made between the three- and five-region results. An example is presented in Reference 1 for a typical ZrH fuel element and a heater element. It was determined that a test rod with a low thermal conductivity region adjacent to the cladding (i.e., a small k_F/k_w^* ratio) would be desirable to closely simulate the effects of

*Refer to Nomenclature List for terms used in text.

the ZrH fuel element gas gap. Since the thermal conductivity of porous magnesium oxide is relatively low, it was used as the electrical insulator for the heater rods. The ratio of cladding-to-coolant thermal conductivities (k_w/k_f) and relative cladding thickness $[(R - r_3)/R]$ are other important parameters involved in fuel element simulation. It was determined that the combination of Type 304 stainless steel cladding and NaK-78 coolant for a heater rod would closely match the conductivity ratio of either Hastelloy X or Inconel 800 and NaK-78 for a ZrH fuel element. To simulate the thin cladding wall thickness range (0.010 to 0.030 in.) of interest to a ZrH fuel element, a 0.020-in. wall was chosen for the stainless steel tubing used for the heater cladding. By careful selection of the parameters $[k_F/k_w, k_w/k_f, (R - r_3)/R]$, as explained previously, a heater element design was determined which simulates the thermal behavior of a ZrH fuel element, within 10%, under identical flow, heating, and geometrical conditions. A more complete description of the test rods will be given in the next section, where the experimental equipment is described.

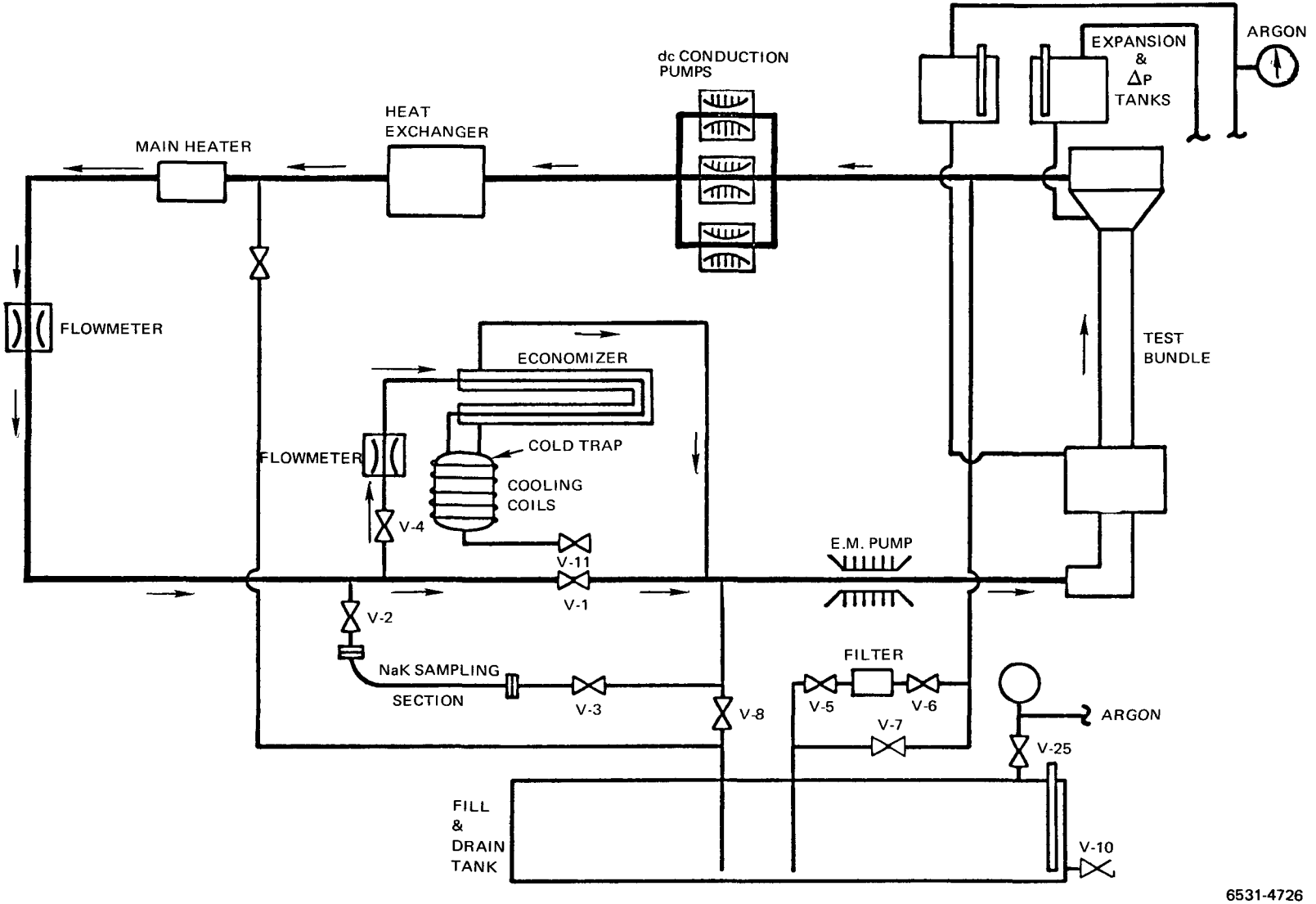

Figure 1. Schematic Flowsheet of NaK Heat Transfer Loop

IV. EXPERIMENTAL EQUIPMENT

A. NaK LOOP

Testing was conducted in a loop facility specifically designed for liquid NaK heat transfer studies. A schematic flowsheet of the loop is shown in Figure 1. The test loop was fabricated with all stainless steel piping and components, and has an all-welded construction. The main loop flow line is made of 1-1/2-in., Schedule 10, Type 316 stainless steel pipe; while the branch lines, such as the fill and drain lines, are made of 1/2-in., Schedule 10, Type 316 stainless steel pipe. Before fabrication of the loop, the piping and components were carefully cleaned with an acetone solution. All welding was done under an argon atmosphere. After fabrication and before filling with NaK, the loop was kept under a positive pressure of pure argon. The entire loop is insulated with at least 3 in. of high-temperature asbestos insulation.

The loop is capable of operating at temperatures up to 1300° F, and flow rates up to 30 gal./min against a 4-1/2 psi head.

Pumping power is supplied by three parallel dc conduction pumps, in series with an electromagnetic linear induction pump. Heat rejection from the loop is accomplished by a 135-kw capacity air blast heat exchanger. A 150-kw in-line NaK heater assembly is located in the main stream of the loop. Flow rates are determined by means of a calibrated permanent magnet flowmeter.

Two expansion tanks, which are also used as surge tanks, are located at the highest point in the loop. The tanks are instrumented to measure the NaK liquid levels and the corresponding pressure drop across the test bundle. Located at the lowest point in the loop is a drain tank which is provided with a 1/2-in. drain line, a 1/2-in. fill line with a 5-μ filter arrangement, and a liquid level probe. System pressure is maintained with argon cover gas, plumbed to both the expansion and drain tanks, with associated pressure gauges, shutoff and vent valves, and a pressure relief valve. The piping is so arranged that pressures in the drain and expansion tanks can be independently controlled.

A flow-through cold trap is located off a 1/2-in. diameter branch line paralleling the main stream line. Water, which serves as the cooling medium, flows

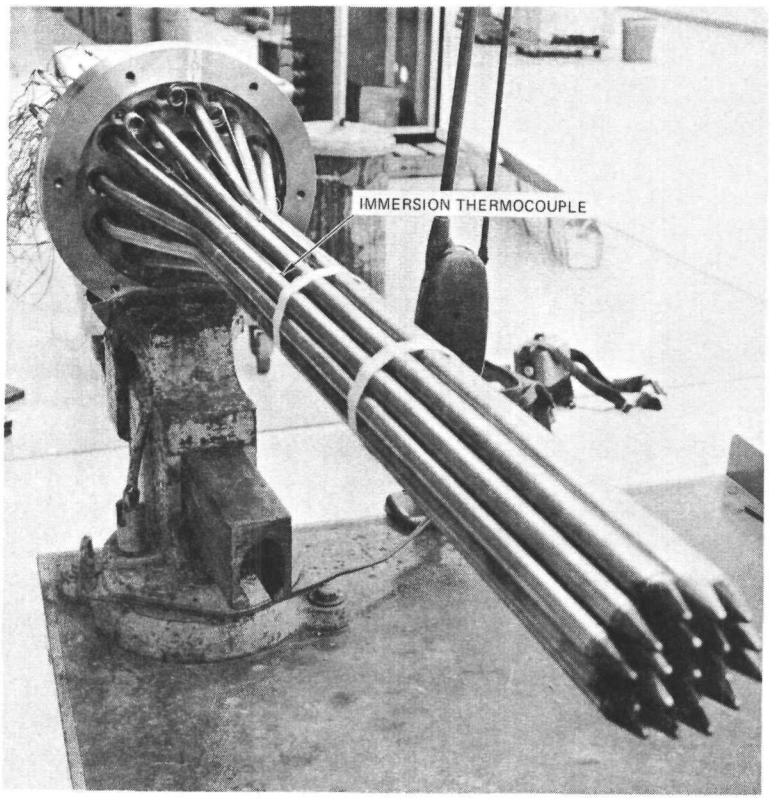

a. Assembly of
19 Heater Elements

7759-40975A

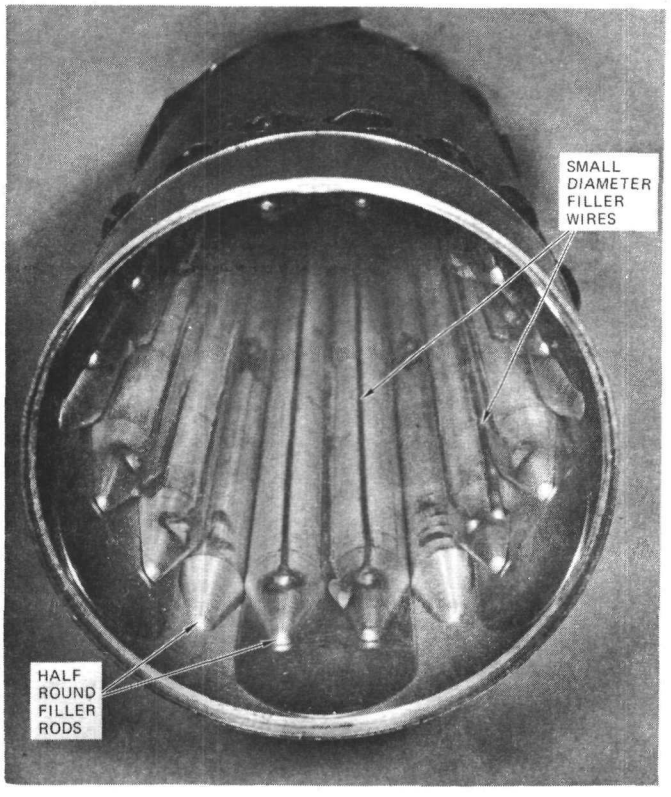

b. Half-Round Filler Rods
and Cylindrical Shell

7759-40766A

Figure 2. Test Section

through 3/8-in. copper tubing which is wrapped around the cold trap. The flow-through method assures that all the NaK eventually passes through the refrigerated region, removing impurities which adhere to the cold surfaces.

In order to perform a periodic chemical analysis of the circulating NaK, a sampling section (1/2-in. OD tube) is located in a branch line, off the main flow line. Isolation valves and Swagelock fittings are provided for easy removal and installation of the NaK sampling tube.

B. TEST SECTIONS

Each test section consisted of a bundle of 19 electrically heated elements, arranged on hexagonal arrays. This bundle of elements was held within a stainless-steel cylindrical shell which had half-round filler rods attached to the inner wall to maintain a proper coolant flow distribution. Figure 2 shows the test section during assembly. For the first test configuration, all neighboring elements were in physical contact, corresponding to P/D = 1.00. The same 19 elements which were used for the first test configuration were used for the second and third test configurations, which were positively spaced with a P/D = 1.05. The second test bundle configuration used ring spacers, 0.562-in. ID by 0.030-in. wall, 1/8-in. wide, to maintain symmetric and positive rod spacing. The ring spacers were banded to each test element (0.562-in. OD) at three different axial locations, as shown in Figure 3. For the third test bundle configuration, 12 of the 19 elements were modified by the addition of helical-fin spacers which were brazed to the outer cladding surface. This spacer configuration is referred to as the right-left-neutral (R-L-N) fin configuration, which means that the fin helix is alternately right hand, left hand, and neutral (no fins), on successive rods throughout the bundle. A sketch of the finned element bundle is shown in Figure 4.

A sketch of a typical heater element, designed to simulate a ZrH fuel element, is shown in Figure 5. It consists basically of a 1/4-in. OD Nichrome coil encased in magnesium oxide (MgO) electrical insulation which is swaged into a 0.020-in. wall, 9/16-in. OD, Type 304 stainless steel tube. Up to 5 kw of power can be supplied to each heater; this corresponds to an outer surface heat flux of 139,000 Btu/hr-ft^2, which is maintained uniformly over the 10-in. heated length. The electrical resistances of all heaters agreed to within 1/2%, and the concentricity and uniformity of the Nichrome coil were confirmed radiographically. As

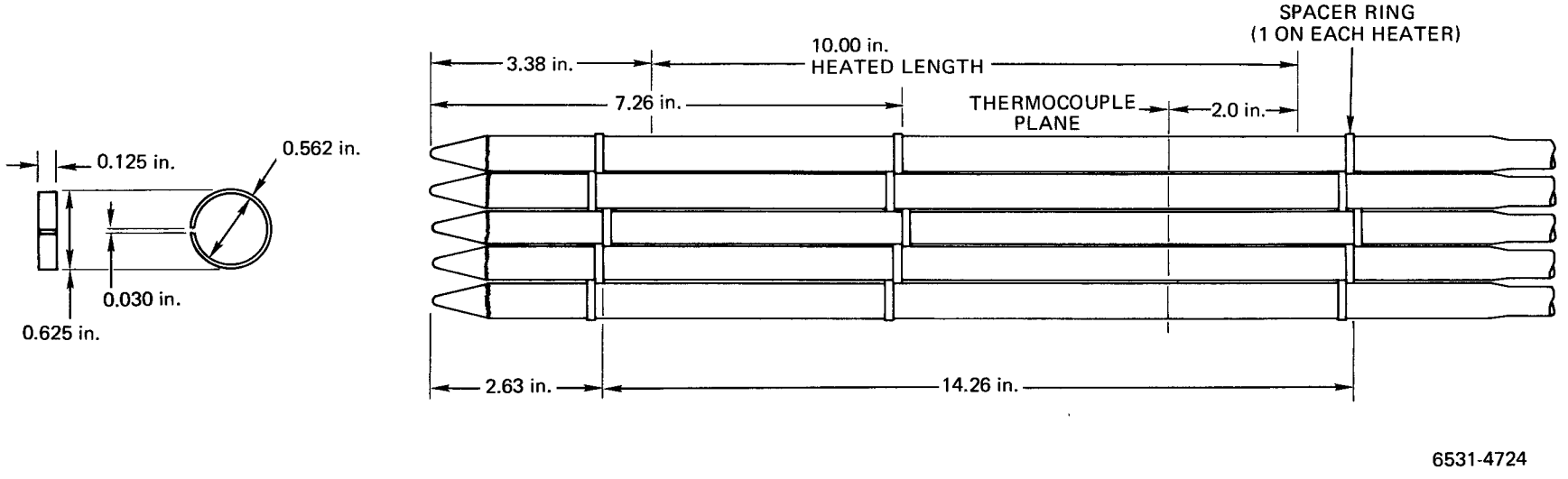

Figure 3. Second Test Configuration, With Ring Spacers

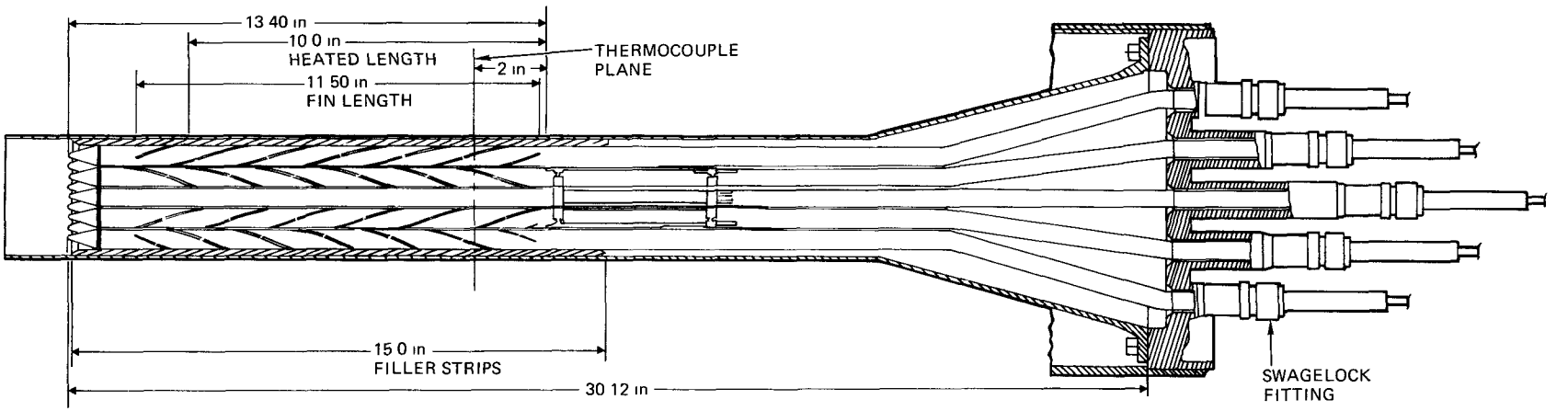

Figure 4. Helical-Fin Spacer Test Configuration

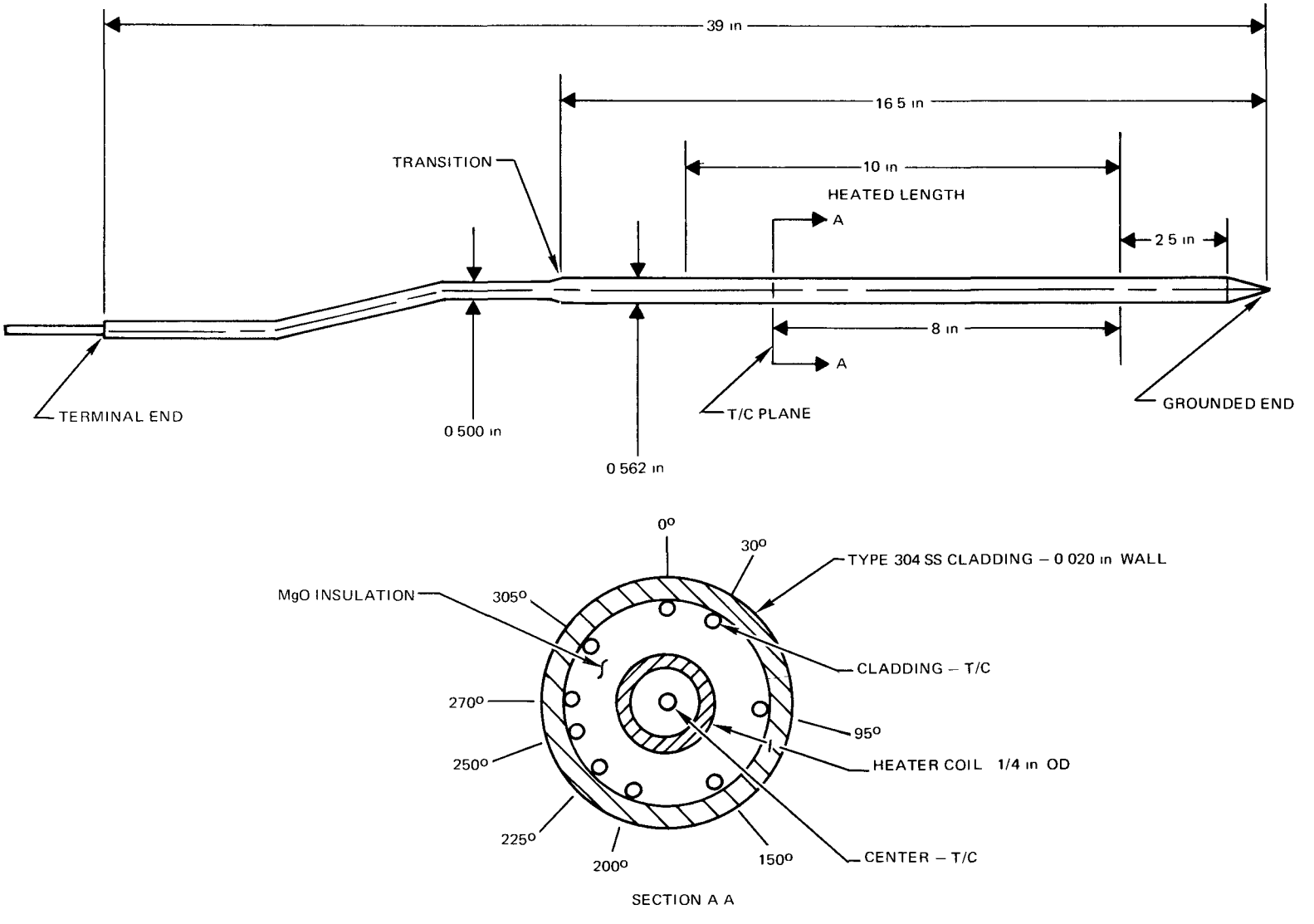

Figure 5. Typical Heat Element

is evident from Figure 5, one end of the elements was swaged down to 1/2-in. OD, and was offset to allow more room for penetrating the test section through standard 1/2-in. Swagelock fittings.

The finned elements, which have either a right-hand or left-hand fin helix, have 3 fins per rod, spaced 120° apart, with an axial pitch of 5.5 in. The fins are 0.030-in. high by 0.060-in. wide. A sketch of a typical finned heater element is shown in Figure 6.

A summary of the test section characteristics for the P/D = 1.00 and 1.05 configurations is shown in Tables 1 and 2 respectively.

C. INSTRUMENTATION

The test rods had small diameter (0.020 in.) thermocouples, flattened to ~10 mils, welded to the inside cladding tube of the test heater. These thermocouples consisted of Chromel-Alumel wires, surrounded by MgO insulation, and sheathed in Inconel 600 tubing. Up to nine thermocouples were accurately located and spaced around the inside cladding periphery at a common axial plane, as shown in Figure 5, to measure the circumferential temperature of the heater cladding.

A cross-sectional view of the rod bundle, showing the relative heater element cladding thermocouple locations, is illustrated in Figure 7. The azimuthal locations are given with respect to the nearest line connecting the centers of adjacent rods. Two of the rods (H-1 and H-4) had eight thermocouples. The other rods had either two or three cladding thermocouples. The cladding thermocouple locations on H-1 through H-7 were chosen to give an adequate mapping of the cladding circumferential temperature distribution, while the locations on H-8 through H-19 were used primarily for rod bundle symmetry checks.

Accurate location of the cladding thermocouples, relative to each other in the test rod bundle, was insured by the following procedure. The thermocouples on each test heater element were circumferentially held in place during welding to the inner cladding wall by a specially designed tool, and the relative angle between thermocouples is accurate to within 2°. A scribe line was placed on the outer surface of each test heater, at a known circumferential location from one of the inner cladding thermocouples. With the use of a template,

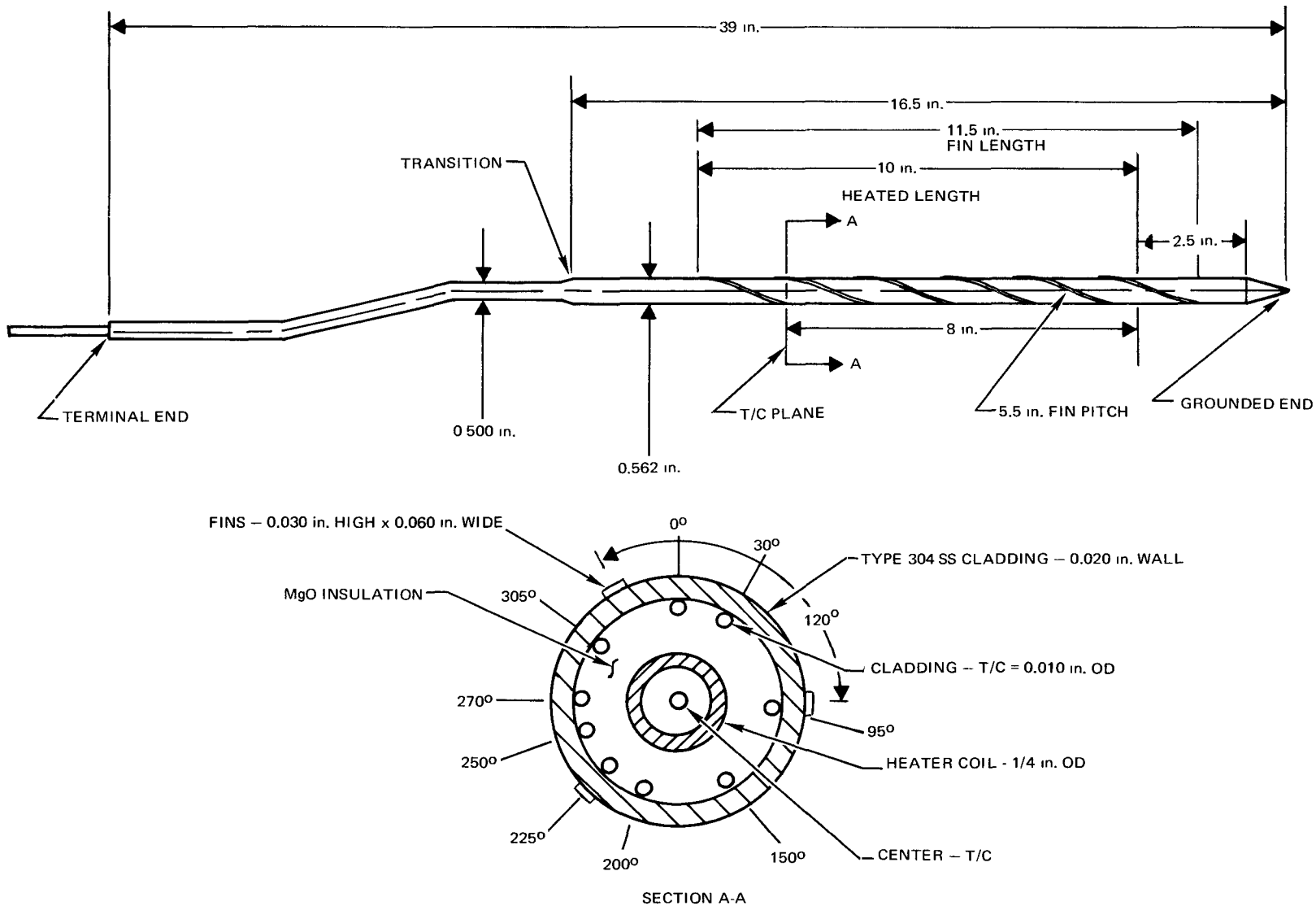

Figure 6. Typical Finned Heater Element

TABLE 1

TEST SECTION CHARACTERISTICS FOR P/D = 1.00

Number of Rods in Bundle	19
Outer Diameter of Rods (in.)	9/16
Geometrical Arrangement	Equilateral Triangular
Length of Rods (9/16-in. OD region) (in.)	16.5
Heated Length (in.)	10.0
Overall Length (in.)	39.0
Pitch-to-Diameter Ratio	1.0
Hydraulic Diameter (in.)	0.0574
Cladding Thermocouple Location With Respect to Velocity Profile Development (z_F/D_h)	183
Cladding Thermocouple Location With Respect to Temperature Profile Development (z_H/D_h)	139

TABLE 2

TEST SECTION CHARACTERISTICS FOR P/D = 1.05

Number of Rods in Bundle	19	
Outer Diameter of Rods (in.)	9/16	
Geometrical Arrangement	Equilateral Triangular	
Lengths of Rods (9/16-in. OD region) (in.)	16.5	
Heated Length (in.)	10.0	
Overall Length (in.)	39.0	
Rod Spacers	Ring Spacer	R-L-N Helical Fin
Spacer Height (in.)	0.030	0.030
Number of Fins per Rod (except neutral rods)	NA	3
Fin Axial Pitch (in.)	NA	5.5
Rod Pitch-to-Diameter Ratio	1.053	1.053
Hydraulic Diameter (in.)	0.1256	0.1095
Cladding Thermocouple Location With Respect to Flow Development (z_F/D_h)	84	96
Cladding Thermocouple Location With Respect to Thermal Development (z_H/D_h)	64	73
Cladding Thermocouple Location With Respect to Middle Spacer Rings (z_S/D_h)	32	NA

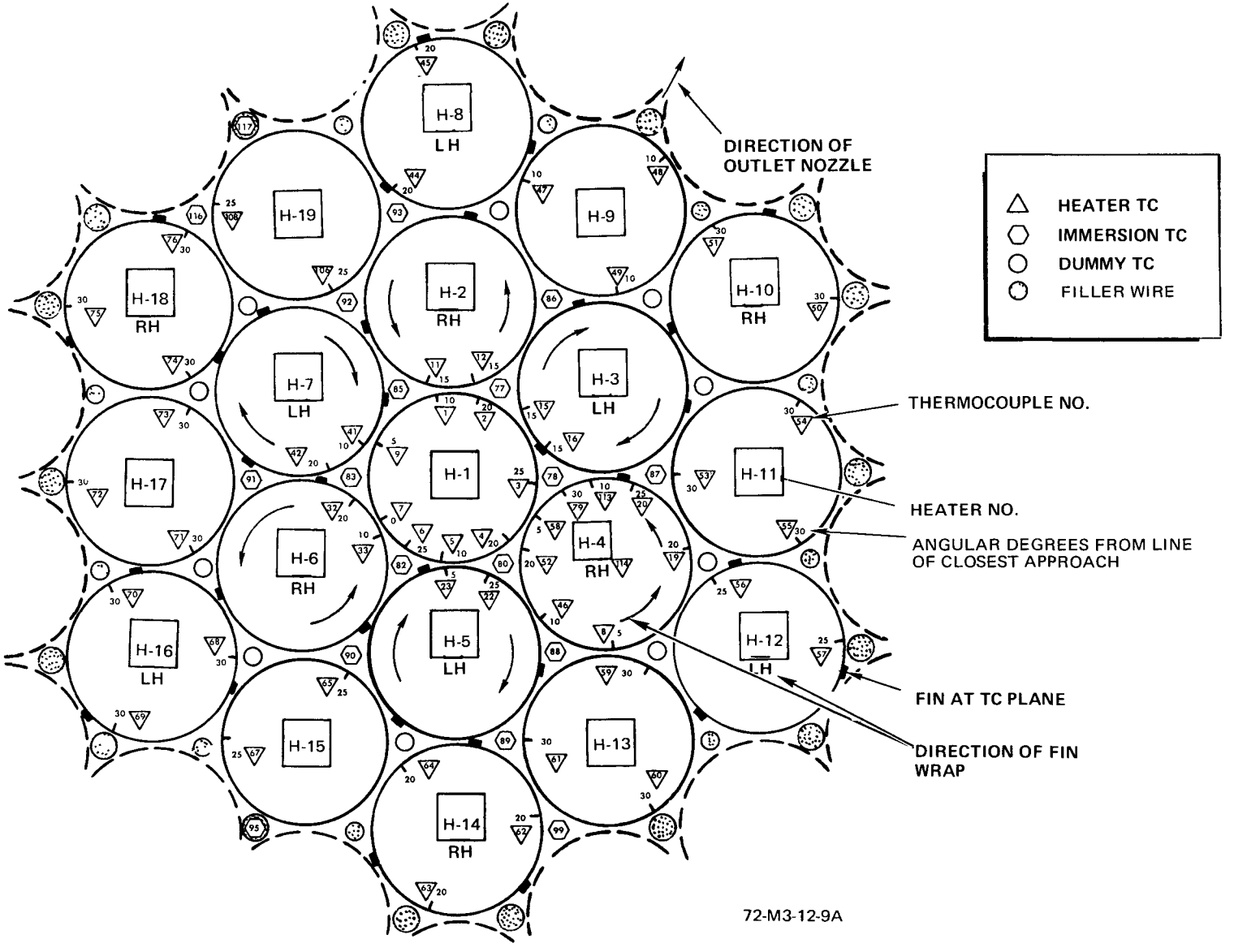

Figure 7. Relative Thermocouple Locations in 19-Rod Bundles

the scribe lines on each test heater element were then located with respect to a fixed reference line, scribed on the test section cylindrical head. It is estimated that the relative circumferential location of thermocouples is accurate to within 5°.

The inner seven rods also had thermocouples installed in the centers of their heating coils, at the same axial location as the cladding thermocouples. The center thermocouples were used to monitor the maximum heater temperatures, and to determine approximately the effective MgO thermal conductivity. Besides providing a check on the uniformity of the heaters, the conductivity determination was useful in providing the k_{MgO}/k_w ratio which was used in the theoretical predictions. As previously mentioned, the k_F/k_w ratio influences the azimuthal temperature and heat flux gradients.

The outlet temperatures of individual tricusp coolant channels were recorded by 1/16-in. OD, Chromel-Alumel thermocouples. Eighteen coolant channels were monitored, and the locations in the rod bundle are also shown in Figure 7. The thermocouples were pointed into, and aligned parallel to, the flow stream. They were held in place by 0.030-in. thick bands which were attached to the heaters. The axial positions of the thermocouples were 0.5 in. downstream from the end of the heated zone. In order to maintain flow symmetry, 1/16-in. OD dummy wires were banded in the same manner at the same axial location, and were located in coolant channels where no thermocouples existed.

The average test section inlet and outlet temperatures were measured by 1/8-in. OD Chromel-Alumel thermocouples. Four thermocouples were inserted in the inlet plenum leading to the test section, and two thermocouples were in the main flow line exiting from the test section.

The NaK flow rate was measured by a dc permanent magnet flowmeter. The flowmeter was calibrated (within an accuracy of 3%) in a NaK flowmeter calibration loop.

The power to each test rod was controlled by separate variable transformers, connected in series with the heaters. The power to each heater element was measured by precision-calibrated ammeter and voltmeter. The accuracy of the power measurement was within 1%.

The emf output of the power controllers, flowmeter, and all test section thermocouples were recorded with a digital data logging system.

V. EXPERIMENTAL PROCEDURE

In order to accurately determine the heat transfer coefficient for a rod bundle geometry, it is important to maintain a uniform coolant temperature distribution across the test section. This can be accomplished by creating the following conditions: (1) a uniform coolant velocity profile at the entrance to the test section, and (2) a proper test section coolant flow distribution. In the present study, the first condition was achieved by the use of a plenum and bellmouth nozzle arrangement at the inlet to the test section. Because of the rapid coolant acceleration, in flowing from the plenum into the bellmouth nozzle, the fluid boundary layer remains attached to the wall, and is relatively thin, causing the pressure loss to be small and the nozzle exit velocity profile to be uniform. The second condition was arrived at by proper sizing of the individual coolant channel flow areas. The peripheral coolant channels, which are adjacent to the half-round filler rods, receive heat from either one or two rods, while the interior channels receive heat from three rods. To keep the bulk coolant temperature rise for the outer edge channels the same as for the interior channels, the mass flow through the peripheral channels had to be reduced in direct proportion to the reduced heat input. This was accomplished by inserting small-diameter filler wires into the outer edge channels (see Figure 7). The wires were sized such that the resulting coolant flow distribution would result in equal coolant temperature rise across the rod bundle.

Since it was the primary objective of the present study to produce dependable data, obtained under carefully controlled conditions, steps were taken to insure that the quantity of dissolved oxides, impurities, and entrained gases were held to a minimum. During inoperative periods, the loop was purged continuously with argon. Prior to filling with NaK, the loop was evacuated to an absolute pressure of 3 μ . With the NaK at room temperature, the loop was loaded by pressurizing the drain tank. In addition, the NaK was routed through a 5-μ micrometallic filter. The fill line in the drain tank was low enough, and the residual NaK level was kept high enough, to minimize the intake of gas or any floating oxides.

While the NaK was circulating through the loop, $\sim$10% of the flow was continuously diverted through a cold trap. The minimum temperature of the cold

trap was held to 100° F. Chemical analysis on hot NaK samples, taken periodically throughout the test, verified that the oxygen concentration was held to 5 ppm or less.

All thermocouples, including those on test heater cladding, test section inlet and outlet, and individual coolant channels, were calibrated before the test, and checked periodically during the test while the NaK was circulated isothermally at various temperatures. Maximum discrepancy between any two thermocouples was <2° F. A digital data logging system, which was used to record the data, was equipped with special devices to filter out any ac noise pickup (ac noise pickup by the thermocouples was determined to be negligible).

The resistances of the heater elements were checked periodically throughout the test. The calibrations of the precision ammeters and voltmeters, used for measuring the power input to all 19 test heaters, were also checked from time to time during the investigation.

Prior to making a run, the flow rate was set, the test heaters were adjusted to the same power level (within 1%), and the test section inlet coolant temperature was allowed to come to a predetermined equilibrium value (within 1° F). Before taking data, sufficient time was allowed to reach steady-state conditions. Although the time to reach equilibrium depended on flow rate and temperature, it was usually <30 min. To verify that the consistency of the data was good, several runs were made at any one particular set of conditions before going on to the next set. In addition, after proceeding through the complete range of conditions, many repeat runs were made.

The scope of the experimental study is presented in Table 3.

TABLE 3
SCOPE OF EXPERIMENTAL STUDY

NaK Temperature Range (° F)	400 to 800
Heat Flux Range (Btu/hr-ft^2)	27,800 to 111,300
Reynolds Number Range	5,000 to 30,000
Prandtl Number Range	0.0067 to 0.0115
Peclet Number Range	35 to 240
Flow Direction	Vertically upward

The NaK was circulated continuously through the loop, even when no power was supplied to the heater elements or when testing was not taking place, such as nights and weekends. The NaK flow was stopped only when it came time to disassemble the test section. At that time, the NaK was dumped at 400° F by pressurizing the surge tank. The NaK was stored in the sealed drain tank until it was time to load the loop for another test configuration.

The physical property values of the NaK-78 used in the study, are as listed in the Sodium-NaK Supplement of the Liquid-Metals Handbook.[13]

VI. EXPERIMENTAL RESULTS

For the three rod bundle configurations, experimental heat transfer results will be presented for the cladding circumferential temperature distributions and the rod-average film coefficients. These results will be presented over a range of heating and flow conditions of interest to compact ZrH reactor cores. In addition, results will be presented which illustrate the effect of rod-spacer-induced inter-channel mixing, or crossflow.

A. CLADDING THERMOCOUPLE MEASUREMENTS

The rod circumferential temperature distributions will be presented in terms of the local cladding temperature above the bulk coolant temperature $[T_{wi}(\theta) - T_b]$. The local inside wall temperatures, $T_{wi}(\theta)$, are determined by thermocouples (T/C) which are welded to the inside cladding tube at selective azimuthal locations. The bulk coolant temperature (T_b), which is subtracted from the local azimuthal temperature, is the average NaK temperature at the heater thermocouple plane, $z_H/L_H = 0.80$. T_b is determined from the average inlet temperature, the average of the individual outlet coolant channel temperatures surrounding the inner seven test heaters (T/C No. 77 through 93, Figure 7), and the measured power supplied to each heater. The individual coolant channel temperatures, as recorded by T/C No. 77 through 93, were within 2° F of being uniform. All 19 heaters were operated at the same power level, and the heat flux was uniform in the axial direction. Heat balances made for various conditions (power, flow rate, and temperature) indicated that test section heat losses were <1%. Since the heaters are arranged on hexagonal arrays, the circumferential temperature profiles repeat every 60°, and are symmetrical with respect to each 30° interval; therefore, the angle θ in the following figures lies in the range $0° \leq \theta \leq 30°$, and is measured from a cladding thermocouple to the nearest line connecting the centers of adjacent heaters.

The circumferential temperature variations on the center test heater (H-1) for the P/D = 1.00 rod bundle, as determined by its eight thermocouple measurements, are shown on Figure 8. The figure clearly illustrates the relatively large azimuthal temperature gradients which exist for a tightly packed rod bundle.

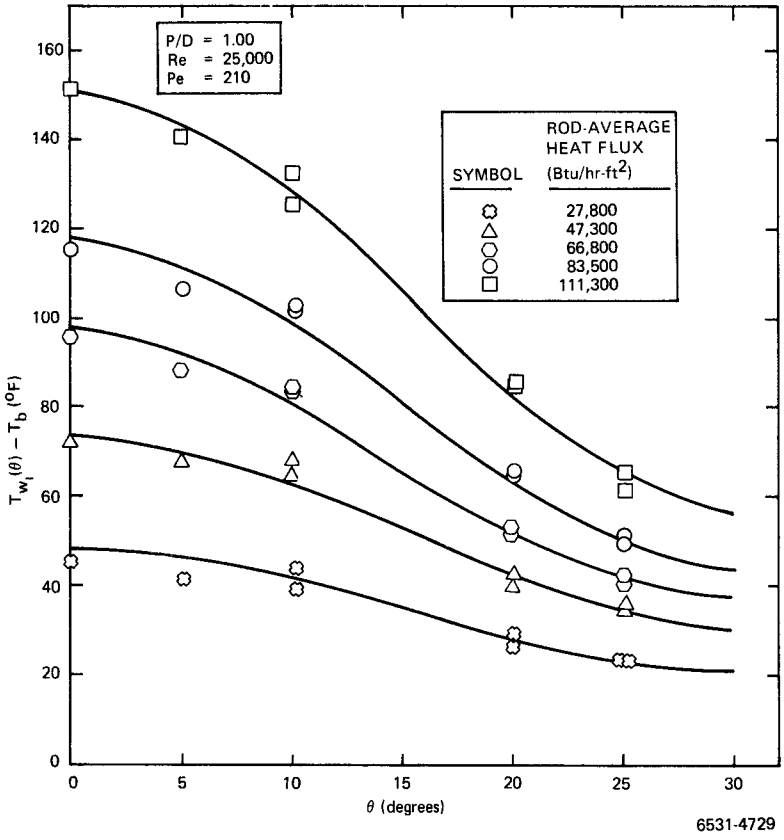

Figure 8. Circumferential Temperature Variations as Measured by Thermocouples on H-1 for the P/D = 1.00 Test

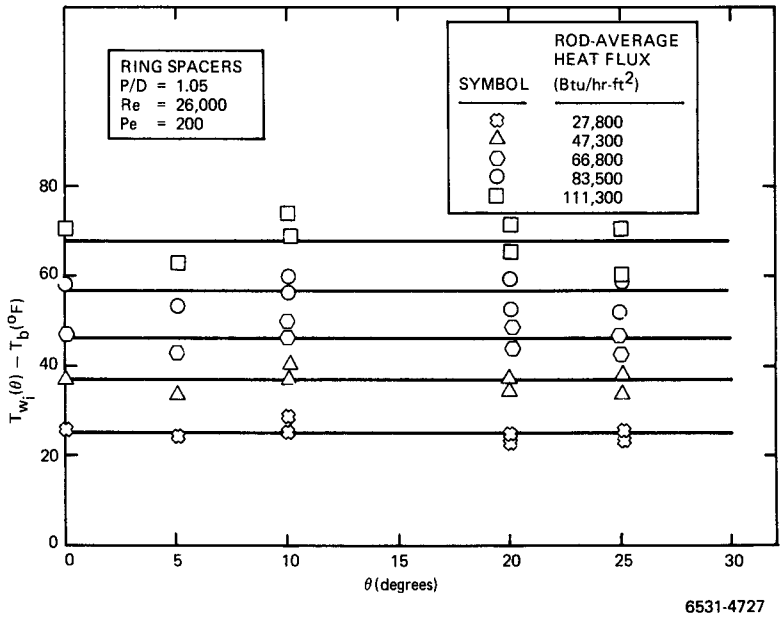

Figure 9. Circumferential Temperature Distribution, as Measured by Thermocouples on H-1 for the Ring Spacer Test Configuration

For the P/D = 1.05 rod bundle configurations Figures 9 and 10 present the circumferential temperature distributions on (H-1) for the ring spacer and helical-fin configurations, respectively. The straight lines drawn through the data points represent mean values. Only a small amount of data scatter is evident. The lack of azimuthal temperature variation for both rod spacer configurations, shown in Figures 9 and 10, are markedly different from the large azimuthal temperature variations shown in Figure 8 for the P/D = 1.00 rod bundle. It will become more evident, later, that the uniformity of the rod azimuthal temperature can be attributed to the effects of positive rod spacing and the increased fluid turbulence and mixing created by the rod spacers.

For the three rod bundle configurations, Figures 11, 12, and 13 present data for the azimuthal temperature distributions, as recorded by thermocouples on the inner seven test rods (H-1 through H-7). By referring to Figure 7, the relative thermocouple locations in the 19-rod bundle can be found. Thermocouples attached to H-3 and H-5 (see Figure 7) were giving erroneous readings, and were not plotted. For the P/D = 1.00 rod bundle, Figure 11 shows that large azimuthal temperature variations, similar to that shown for the central rod, existed on the inner seven rods of the 19-pin bundle. For the P/D = 1.05 rod configuration, horizontal straight lines represent the best fit to the data, shown in Figures 12 and 13, and are drawn through the mean of the data points. These data indicate that no azimuthal temperature variations existed on any of the inner seven rods in the 19-rod bundle test configurations. Comparing the data shown in Figures 11 through 13 to that shown in Figures 8 through 10 for the center rod indicates that, although the mean values of the two sets of data are approximately the same, more data scatter exists for temperatures recorded by thermocouples on the inner seven test rods. The increased data scatter can be attributed to fabrication nonuniformities of the heater elements, inaccuracy of thermocouple locations to within 5°, and slight deviations from a perfectly symmetrical rod arrangement. It should be noted, however, that the data scatter evident in Figures 11 through 13 is really not large for this type of investigation.

In addition to obtaining data over a range of heat flux values, circumferential temperature distributions were measured for various Reynolds numbers, or Peclet numbers, of interest to compact ZrH reactor cores. For the center test rod (H-1), Tables 4 through 6 present data for the local temperature above the bulk coolant temperature for the three rod bundle configurations.

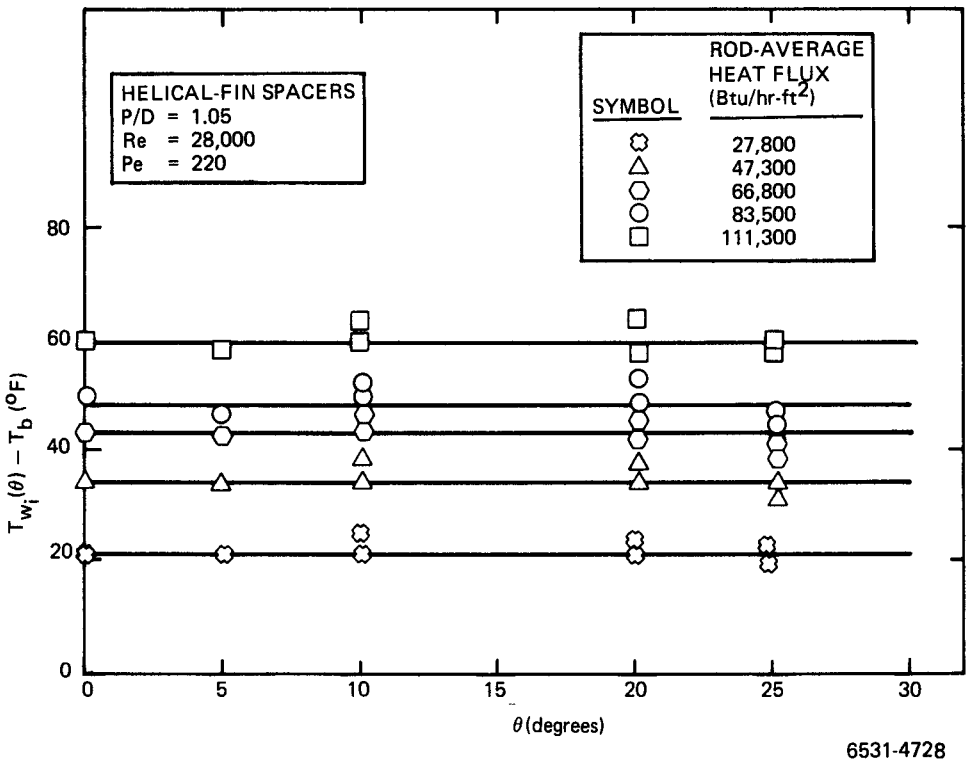

Figure 10. Circumferential Temperature Distribution, as Measured by Thermocouples on H-1 for the Helical Fin Test Configuration

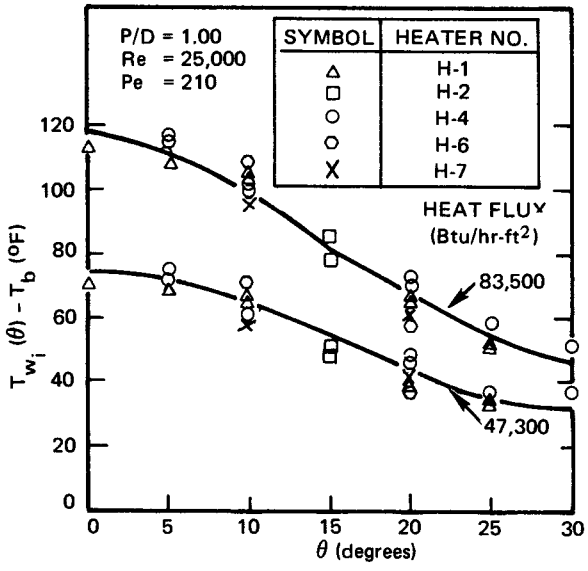

Figure 11. Circumferential Temperature Variations, as Measured by Thermocouples on the Inner Seven Rods (H-1 through H-7)

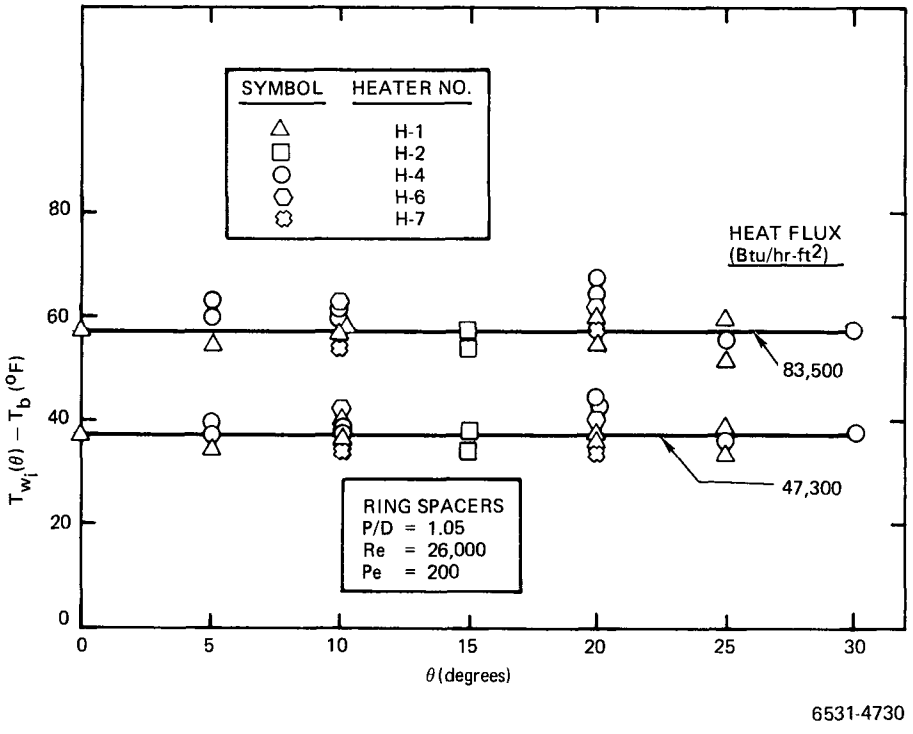

Figure 12. Circumferential Temperature Distributions, as Measured by Thermocouples on H-1 Through H-7 for the Ring Spacer Test Configuration

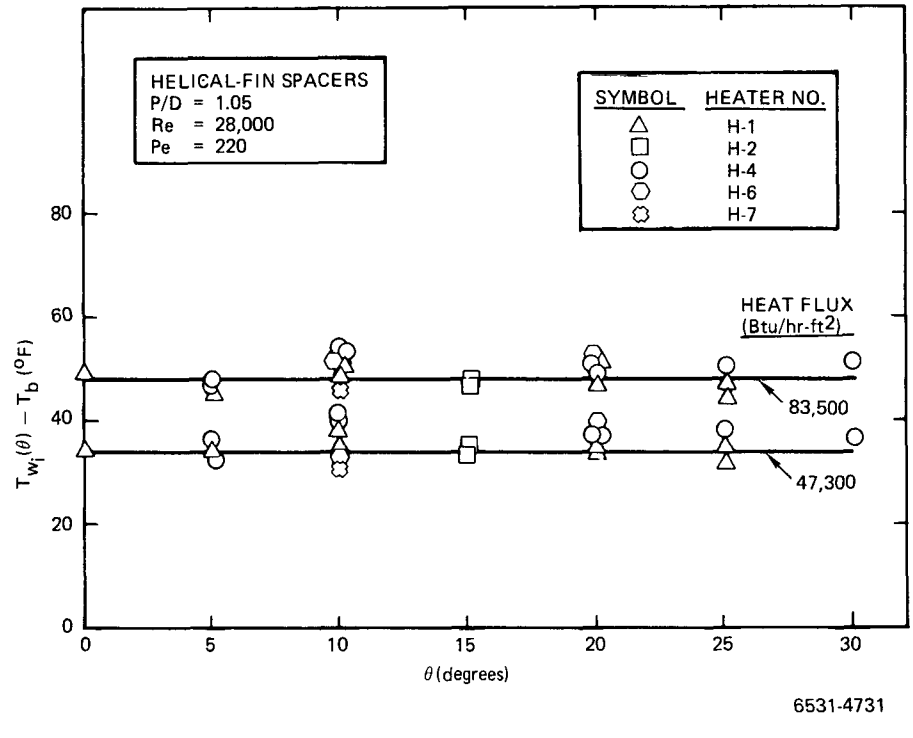

Figure 13. Circumferential Temperature Distributions, as Measured by Thermocouples on H-1 Through H-7 for the Helical-Fin Test Configuration

TABLE 4

LOCAL CLADDING TEMPERATURE ABOVE THE BULK COOLANT TEMPERATURE FOR VARIOUS PECLET NUMBERS

θ (°)	$T_{w_i}(\theta) - T_b$ (°F)					
	Re = 26,000 Pe = 205	Re = 20,000 Pe = 155	Re = 15,000 Pe = 115	Re = 11,000 Pe = 80	Re = 7,600 Pe = 58	Re = 5,300 Pe = 38
	$\overline{q''}$ = 27,800 Btu/hr-ft^2					
0	45.8		46.7	46.5	46.0	47.6
5	41.8		42.4	41.8	41.8	41.7
10	44.0		43.3	44.0	43.5	43.4
	40.2		41.1	42.3	42.6	43.7
15	-		-	-	-	-
20	27.6		27.4	28.2	28.3	29.0
	25.5		25.7	27.0	26.6	26.9
25	24.2		23.1	23.1	22.4	22.7
	22.9		22.7	23.1	23.2	24.4
30	-		-	-	-	-
	$\overline{q''}$ = 47,300 Btu/hr-ft^2					
0	72.0	71.8	72.5	73.8		
5	67.8	67.6	67.5	68.3		
10	68.2	67.6	68.4	70.0		
	66.2	65.9	67.5	69.8		
15	-	-	-	-		
20	42.7	42.6	43.6	43.8		
	39.7	39.7	39.3	40.3		
25	35.8	35.4	34.3	32.8		
	33.7	33.3	33.4	33.6		
30	-	-	-	-		

TABLE 5

LOCAL CLADDING TEMPERATURE ABOVE THE BULK COOLANT TEMPERATURE FOR VARIOUS REYNOLDS NUMBERS OR PECLET NUMBERS, RING SPACER CONFIGURATION

$\overline{q''}$ = 46,700 Btu/hr-ft^2

θ (°)	$T_{w_i}(\theta) - T_{b_i}$ (°F)				
	Re = 29,800 Pe = 240	Re = 25,300 Pe = 200	Re = 19,500 Pe = 150	Re = 14,800 Pe = 110	Re = 10,300 Pe = 75
0	35.6	36.4	37.2	39.6	41.0
5	33.8	33.8	33.8	34.9	34.4
10	40.3	40.7	40.6	40.4	39.0
	36.0	36.8	37.6	41.3	42.8
15	-	-	-	-	-
20	34.7	35.1	34.2	35.5	33.1
	35.6	36.4	35.9	37.9	39.4
25	38.1	38.6	38.9	40.4	41.0
	33.4	33.8	33.3	34.5	34.8
30	-	-	-	-	-
$\overline{T_{w_i}(\theta) - T_{b_i}}$	35.9	36.5	36.4	38.0	38.2

TABLE 6

LOCAL CLADDING TEMPERATURE ABOVE THE BULK COOLANT TEMPERATURE FOR VARIOUS REYNOLDS NUMBERS OR PECLET NUMBERS, HELICAL-FIN SPACER CONFIGURATION

$\overline{q''}$ = 46,700 Btu/hr-ft^2

θ (°)	$T_{w_i}(\theta) - T_{b_i}$ (°F)				
	Re = 27,600 Pe = 220	Re = 22,600 Pe = 180	Re = 17,600 Pe = 140	Re = 13,200 Pe = 100	Re = 9,100 Pe = 70
0	35.0	35.3	35.1	35.7	36.3
5	32.7	31.1	31.7	32.0	31.0
10	32.9	31.5	31.5	32.1	31.4
	38.3	38.5	38.8	40.2	40.3
15	-	-	-	-	-
20	37.7	37.6	37.3	37.5	37.9
	32.3	32.5	32.7	32.8	33.1
25	32.3	30.3	30.2	31.8	30.0
	31.2	29.5	29.1	29.8	29.8
30	-	-	-	-	-
$\overline{T_{w_i}(\theta) - T_{b_i}}$	34.1	33.3	33.3	34.0	33.7

As is evident from Table 4, there is essentially no Pe dependence over the range investigated for the P/D = 1.00 rod bundle. The Pe independence was expected, since the data were obtained in the low turbulent flow regime, where the eddy thermal diffusivity is negligible, compared to the molecular diffusivity for a liquid metal. For the ring spacer configuration (P/D = 1.05) results presented in Table 5, there is negligible circumferential temperature variation; however, the average value of $[T_{w_i}(\theta) - T_b]$ does show a slight Pe dependence over the flow range investigated. As shown later, the preceding flow dependence will be reflected in the results for the rod-average film coefficients. Although the flow dependence is small, it does exist, and is most likely due to a Re dependence of the increased fluid turbulence and mixing created by the ring spacers. For the helical-fin spacer configuration, as is evident from Table 6, there is essentially no Pe dependence over the range investigated ($35 \leq Pe \leq 220$).

Referring to Figure 3, it should be pointed out that the middle spacer rings were ~30 hydraulic diameters from the axial plane of the cladding thermocouples. For closely spaced ($P/D \leq 1.10$) rod bundles, the results of Zhukov et al.[14] indicate that 60 to 100 hydraulic diameters may be required to establish fully developed temperature profiles. The uniformity of the cladding temperature distributions, shown in Figures 9 and 12, can be attributed to the flow disturbance created by the middle spacer rings. Apparently, a significant increase in the fluid turbulence intensity results, downstream of the ring spacers. From the results shown in Table 5, the flow disturbance created by the middle spacer rings has a slight Re dependence, similar to that observed at the entrance region to a flow channel. For the helical-fin spacer configuration, the fins are distributed along the entire length of the heated region, resulting in a more continuous flow disturbance. Although the increased turbulence intensity is significant to negate any rod circumferential temperature gradient, the indicated independence on Re is apparently due to the continuous nature of the flow perturbation, unlike the ring spacers, which represent a sudden change in the flow characteristics.

B. COMPARISON OF THEORY AND EXPERIMENT FOR THE INNER CLADDING WALL TEMPERATURE DISTRIBUTION

In order to compare experimental results with theoretical predictions for the inside cladding circumferential temperature distributions, the thermocouple measurements on the center test rod, shown in Figures 8 through 10, had to be corrected to determine the true inner cladding wall temperature. The thermocouples, which are welded to the inner cladding tube, were recording temperatures which corresponded to a ~5-mil depth into the MgO insulation of the heater. This is not surprising, in view of the fact that the effective thermocouple thickness is 10 mils, and there exists a large radial temperature gradient (~4° F/mil) through the MgO. As was explained in detail in Reference 2, radial temperature correction factors, which are shown in Figure 14 for convenience, were determined from single-heater NaK calibration tests. These tests were performed on the center test heater (H-1), under conditions of NaK annular flow. By testing under uniform, well-described heat transfer conditions, the true inner cladding wall temperature could be calculated accurately, and compared to measured values. The results, shown in Figure 14, represent the difference between true and measured values for the inner cladding wall temperatures. The results were determined over the same temperature and heat flux range as covered in the 19-rod bundle studies.

After the radial temperature correction factors were applied to the results shown in Figures 8 through 10, experimentally corrected inner cladding wall temperature distributions were determined for the various test configurations as shown in Figures 15a and b. Predicted results for the inner cladding azimuthal temperature variation are also shown in these figures for comparison. As previously mentioned, the theoretical results were determined from an analytical model developed for P/D = 1.00, and modified for the case of P/D = 1.05. The predicted results were determined for values of the parameters P/D, k_F/k_w, k_w/k_f, and $(R - r_3)/R$, corresponding to conditions of the present experimental study. The k_F values which were used in the calculations are those corresponding to the experimental values of k_{MgO}. For the P/D = 1.00 rod configuration, Figures 15a and b show good agreement between the predicted and experimentally corrected results, while Figures 16 and 17 show poor agreement for the P/D = 1.05 configuration. The poor agreement can be attributed to the fact that the

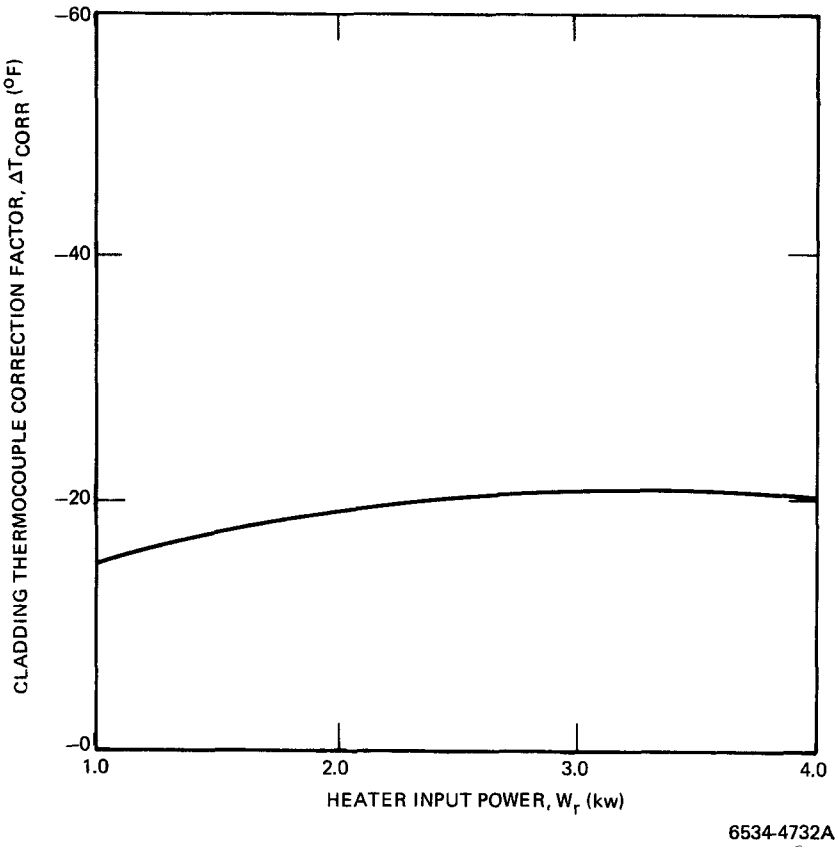

Figure 14. Radial Temperature Corrections for Inside Cladding Thermocouples, as Determined from Single-Heater NaK Calibration Test on H-1

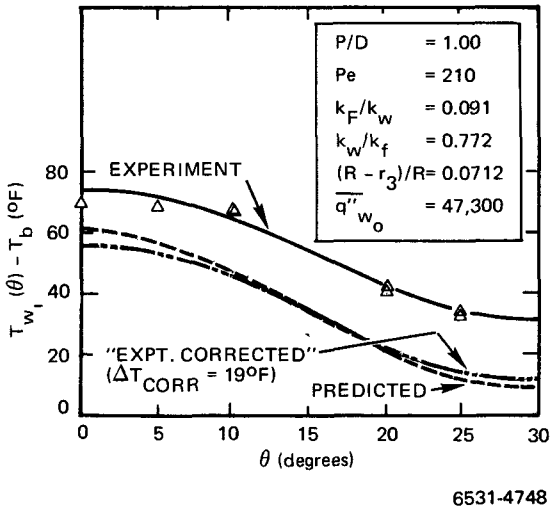

a. $\overline{q''}_{w_o}$ = 47,300 Btu/hr-ft^2

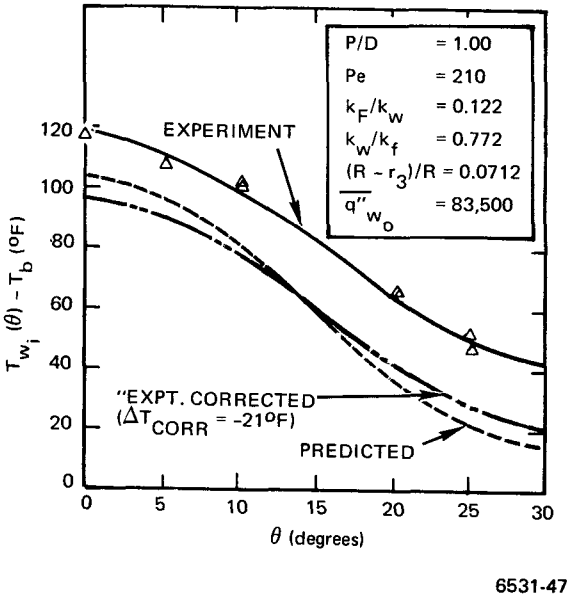

b. $\overline{q''}_{w_o}$ = 83,500 Btu/hr-ft^2

Figure 15. Comparison of Theory and Experiment for Inside Cladding Circumferential Temperature Variation for H-1

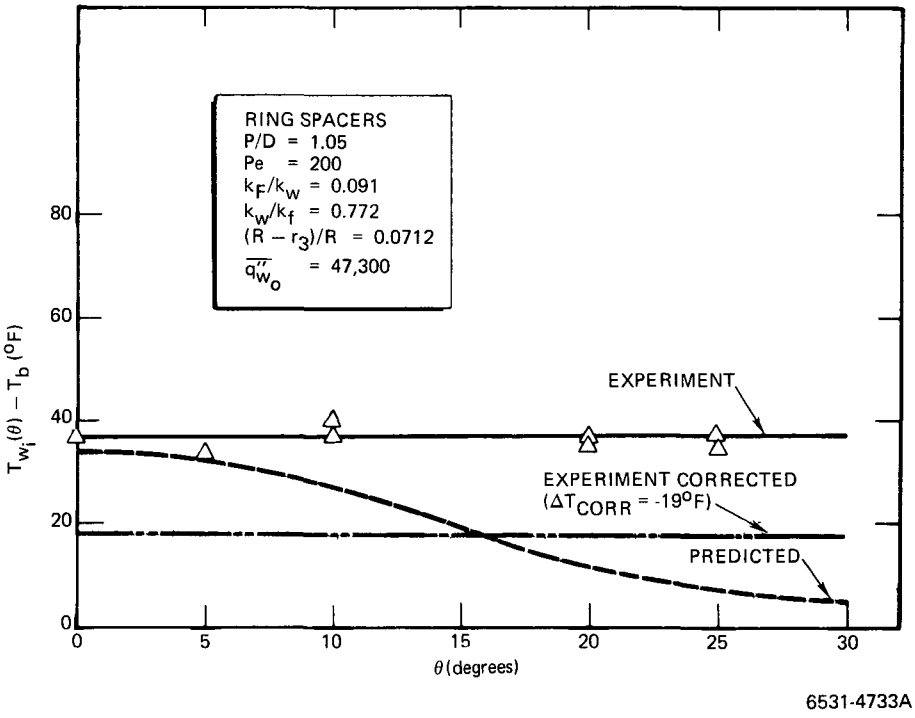

a. $\overline{q''}_{w_o}$ = 47,300 Btu/hr-ft^2

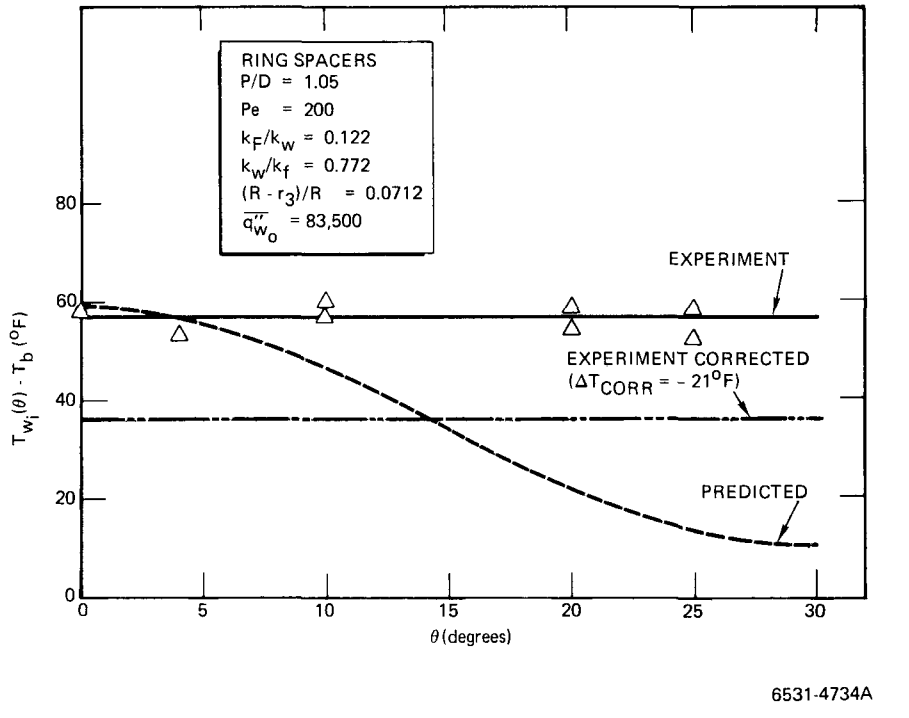

b. $\overline{q''}_{w_o}$ = 83,500 Btu/hr-ft^2

Figure 16. Comparison of Theory and Experiment for the Inside Cladding Circumferential Temperature Variation on H-1 for the Ring Spacer Test Configuration

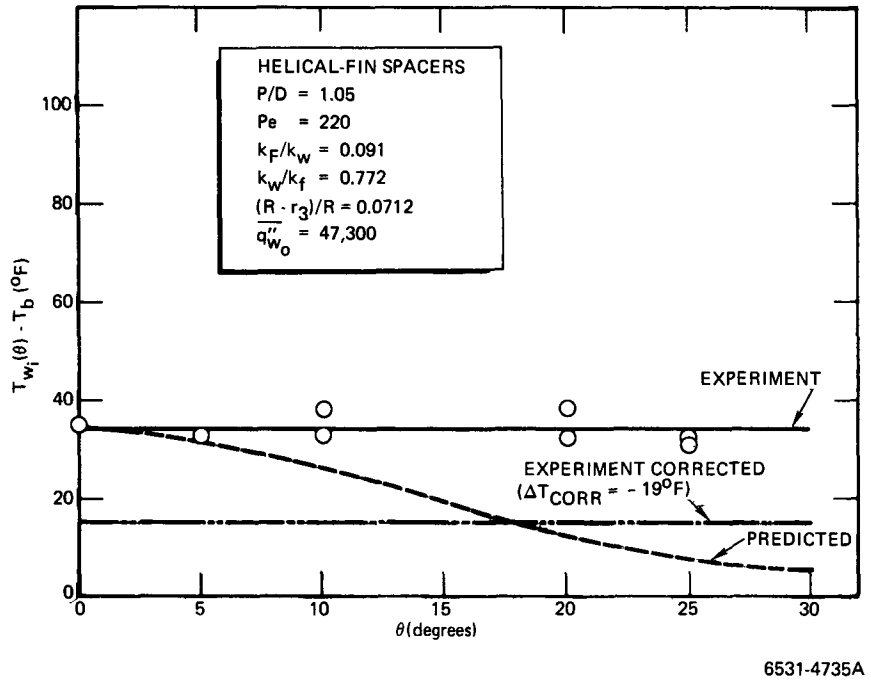

a. $\overline{q''}_{w_o}$ = 47,300 Btu/hr-ft^2

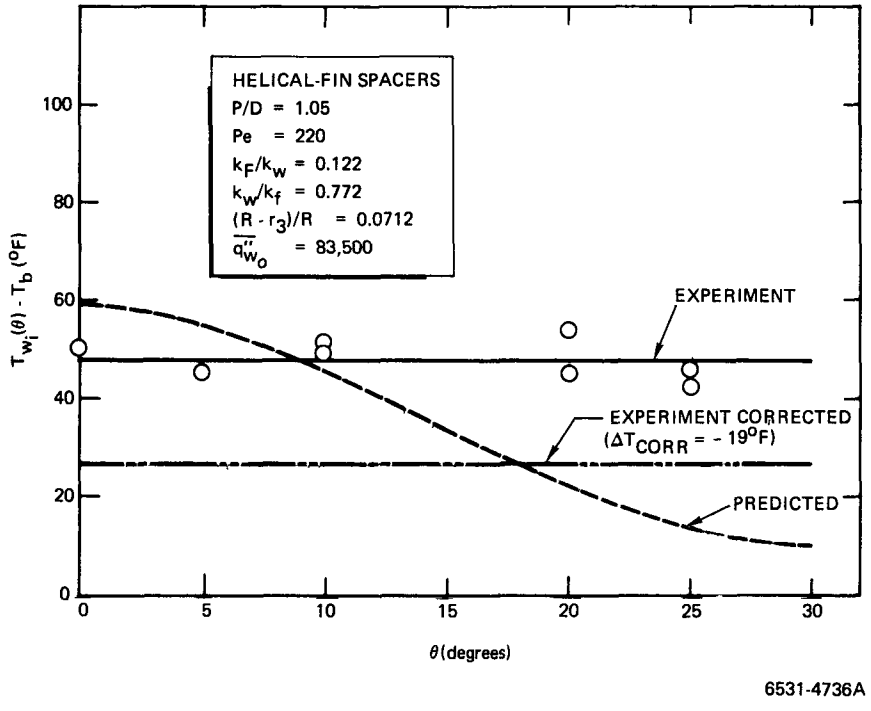

b. $\overline{q''}_{w_o}$ = 83,500 Btu/hr-ft^2

Figure 17. Comparison of Theory and Experiment for the Inside Cladding Circumferential Temperature Variation on H-1 for the Helical-Fin Test Configuration

predicted results were obtained from a smooth tube analytical model, which does not account for the increased turbulence and mixing effect of rod spacers. Since the theoretical results are considered to be quite accurate for the case of smooth tubes, the comparison does show the reduction of the azimuthal temperature variation caused by the ring and helical-fin type rod spacers.

From the test results, it can be shown that, for closely spaced, smooth tube bundles, the average inside cladding wall temperature ($\overline{T}_{w_i}$) is very nearly equal to the local wall temperature at $\theta = 15°$; that is,

$$\overline{T}_{w_i} = \frac{1}{\pi/6}\int_0^{\pi/6} T_{w_i}(\theta)\,d\theta = T_{w_i}(\theta = 15°) \quad . \qquad \ldots(1)$$

This relationship is also valid for the outside cladding wall temperature distribution $\left[T_{w_o}(\theta)\right]$. For the P/D = 1.00 configuration, Figures 15a and b show that good agreement exists between the predicted and the experimentally corrected values for the average inside wall temperature $\left[T_{w_i}(\theta = 15°)\right]$. It is interesting to note, from the ring spacer test results (P/D = 1.05), shown in Figures 16a and b, that the corrected inside wall temperature is approximately the mean value of predicted azimuthal variation. This indicates that the presence of the spacer rings, while negating the circumferential temperature gradient, had essentially no influence on the average cladding temperature. Apparently, the increase in the intra-channel turbulence intensity is primarily in the azimuthal direction, with little influence on the radial component. For the helical-fin configuration results, shown in Figures 17a and b, the predicted average cladding temperature is considerably above the measured value, indicating that the helical fins caused increased radial, as well as azimuthal, intra-channel mixing. As will be shown in the following section, the preceding comparisons between theoretically predicted and experimental average inside cladding wall temperature ($\overline{T}_{w_i}$) will have an important bearing on similar comparisons for the rod-average heat transfer coefficient.

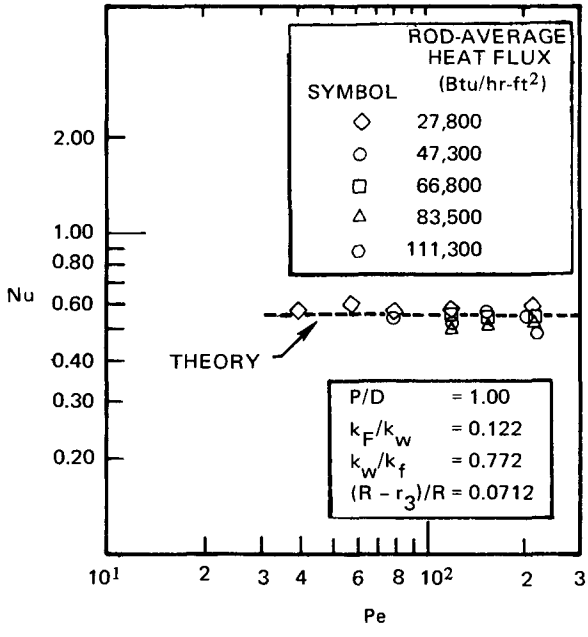

6531-4715A

Figure 18. Comparison of Theory and Experiment for the Rod-Average Nusselt Number Variation with Peclet Number

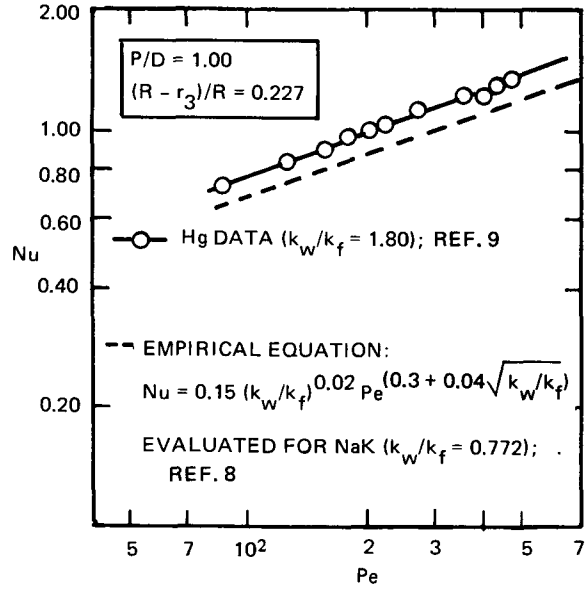

6531-4716A

Figure 19. Experimental Nusselt Number Variation with Peclet Number, Taken from the Works of Subbotin et al.[8, 9]

C. ROD-AVERAGE HEAT TRANSFER COEFFICIENT

Experimental values for the rod-average heat transfer coefficient ($\bar{h}$) were determined for the center test rod (H-1). From results such as those shown in Figures 15 through 17, which have been corrected for the radial temperature correction factors of Figure 14, average values of the quantity $[T_{w_i}(\theta) - T_b]$ were determined for various flow and heating conditions. The average outer cladding temperature can then be found from:

$$\overline{T}_{w_o} = \overline{T}_{w_i} - \frac{3413\ W_r \ln (R/r_3)}{2\pi L_H k_w} \quad . \qquad \ldots(2)$$

From measurements of the power supplied to the center test rod and the bulk coolant temperature at $z_H/L_H = 0.80$, the rod-average film coefficient is determined by

$$\bar{h} = \frac{3413\ W_r}{\pi D L_H (\overline{T}_{w_o} - T_b)} \quad . \qquad \ldots(3)$$

For the P/D = 1.00 rod bundle, experimental film coefficient results are shown in Figure 18, in dimensionless form of Nu vs Pe. For conditions corresponding to the present study, and assuming Pe independence, the predicted Nu value is also shown for comparison. The mean of the data points and the theoretical curve coincide. Since the average deviation from the predicted curve is ±5%, the agreement between theory and experiment is considered to be excellent. The predicted value of Nu = 0.560, shown in Figure 18, corresponds to a heat transfer coefficient of $\bar{h}$ = 1750 Btu/hr-ft^2. In the flow range investigated, these experimental results confirm that the Nu values are independent of Pe, unlike the results of Subbotin *et al.*,[8,9] which are shown in Figure 19 for comparison. As previously mentioned, the fact that Subbotin's Nu results exhibit a Pe dependence is probably due to the presence of dissolved oxides or entrained gases. These contaminants result in an added contact resistance at the rod surface which is flow or Pe dependent. This phenomenon is explained in detail by Dwyer in Chapter 5 of Reference 13.

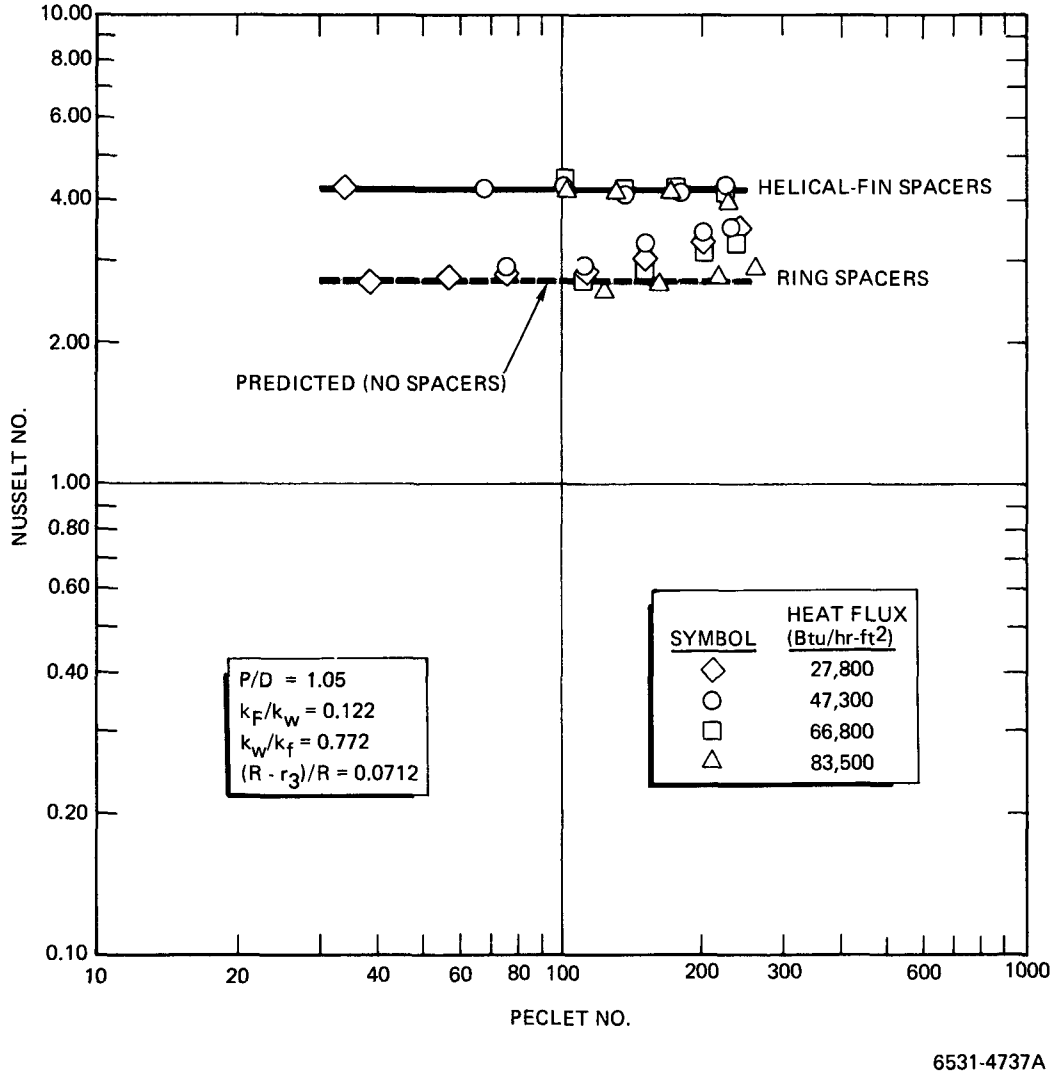

Figure 20. Comparison of Theory and Experiment for the Nusselt Number Variation with Peclet Number for the Ring and Helical-Fin Spacer Configuration

Figure 20 presents experimental results for the Nusselt number variation with Peclet number for positively spaced rod configurations (P/D = 1.05). The predicted smooth-tube Nu value which was determined from the analytical model is also shown. The model assumption of negligible eddy-thermal diffusivities, which is valid in the low turbulent flow regime of this study, results in Nu independence of Pe.

For the ring spacer configuration, good agreement between the experimental and predicted Nu values exists for Pe < 150. For Pe > 150, the experimental values of Nu are 10 to 35% greater than the predicted values, and show a slight Pe dependence. This is consistent with the average inside cladding temperature results, as shown in Table 5. For this type investigation, the preceding 10 to 35% discrepancy is small, and reasonable agreement between theory and experiment is considered to exist over the full Pe range investigated. Therefore, the spacer rings, while negating the cladding azimuthal temperature gradient, had little influence on the rod-average cladding temperature and film coefficient. The predicted value of Nu = 2.74, shown in Figure 20, corresponds to a heat transfer coefficient of $\bar{h}$ = 3930 Btu/hr-ft^2-°F.

For the helical-fin spacer configuration, the experimental Nu values shown in Figure 20 are seen to be independent of Pe, over the range investigated. The mean value of the data points, Nu = 4.20, corresponds to a heat transfer coefficient of $\bar{h}$ = 6900 Btu/hr-ft^2-°F. The average deviation of the data points from the mean value is ±2%. Comparing the theoretical (no spacers) and experimental Nu values indicates that the spiral fins caused ~53% increase in the rod-average film coefficient.

D. COMPARISON OF RESULTS FOR THREE TEST CONFIGURATIONS

For the three rod bundle configurations, Figures 21 and 22 show comparisons for the center-rod azimuthal temperature distributions and the rod-average Nusselt numbers, respectively. The data points for the rod temperature distributions have been corrected from the results of Figure 14. In addition, these figures show the predicted rod temperature variations and Nusselt numbers, based on a smooth tube (no spacers) analytical model. Figure 21 shows that the effect of the ring and fin spacers was to eliminate the rod azimuthal temperature variation. With respect to the rod-average film coefficient (Nu), Figure 22

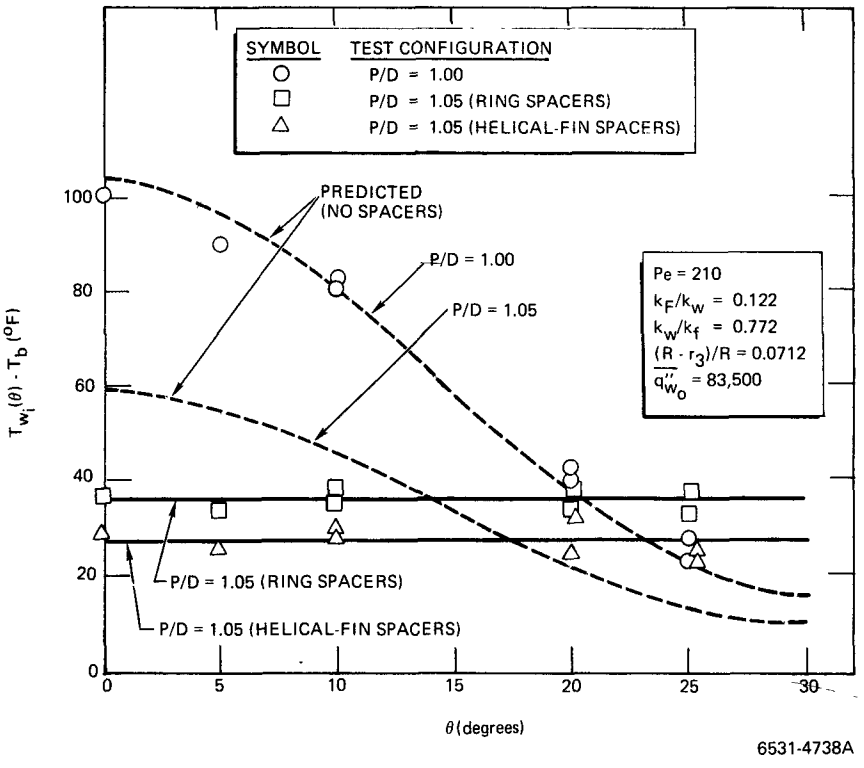

Figure 21. Comparison of Theory and Experiment for the Inside Cladding Circumferential Temperature Variation on H-1 for the Three-Rod Bundle Configuration Examined to Date

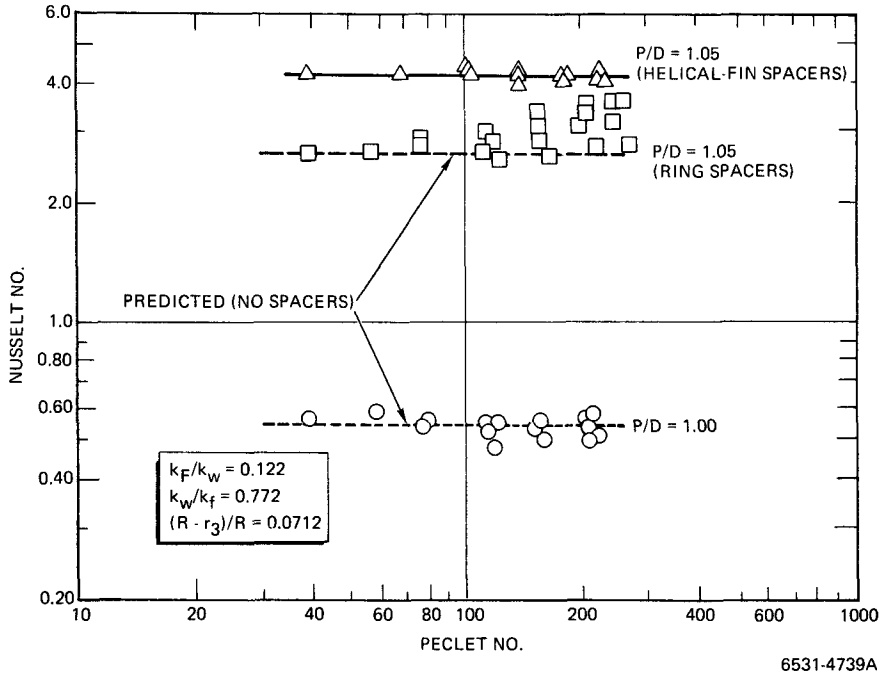

Figure 22. Comparison of Theory and Experiment for the Nusselt Variation with Peclet Number for the Three-Rod Bundle Configurations

shows considerably greater values for the P/D = 1.05 bundles than for the P/D = 1.00 bundle. This is primarily due to the effect of positive rod spacing. Comparing the results shown in Figures 21 and 22 for the two-rod bundles at P/D = 1.05, it is evident that helical-fin spacers resulted in a lower value of the average wall temperature difference $\left[\overline{T_{w_i}(\theta) - T_b}\right]$ and a considerably greater rod-average film coefficient, as compared to the ring spacer results. Since the effects of the spacers is not included in the analytical model, comparison between predicted and experiment is valid only for the smooth-tube (P/D = 1.00) rod bundle configuration.

E. TRANSITION FLOW TEST

An attempt was made to determine the transition Reynolds number (i.e., the Re value at which transition from turbulent to laminar flow takes place). Tests were conducted at low coolant flow rates, corresponding to a Re range of 2000 to 5000. To determine the transition Re, temperature vs time records were obtained from selective cladding and coolant channel thermocouples. At the transition Re, relatively large temperature fluctuations would be observed.

For the P/D = 1.00 rod bundle configuration, Re values in the range of 2000 to 3000 were observed to cause large cladding temperature fluctuations, indicating that operation in the transition zone between turbulent and laminar flow was taking place. The magnitude of the cladding temperature fluctuations was $\sim$50% of the average film temperature drop (ΔT_f), and occurred at a frequency of $\sim$1 Hz. For the P/D = 1.05 test configurations, temperature fluctuations were not observed to occur for Re values down to 2000. Apparently, the presence of the ring spacers and helical fins shifted the transition Re to a value <2000. Operating at Reynolds numbers <2000 was not possible with the available loop configuration.

F. INNER-CHANNEL COOLANT MIXING, OR CROSSFLOW

Besides promoting increased intra-channel turbulence, it was expected that the rod spacers would induce forced inter-channel coolant mixing, or crossflow. Under certain asymmetric geometry conditions, forced crossflow would be important in alleviating the large cross fuel element temperature differences, and resulting bending stresses, that can occur. It was a primary objective of this

study to determine the influence of rod spacers in reducing cross coolant-to-coolant channel temperature differences.

Asymmetric heating tests were performed to determine the extent of coolant channel temperature change due to rod-spacer-induced mixing. The asymmetric heating conditions were produced by turning off selective heaters in the 19-rod bundle. This, in effect, produced temperature differences in adjacent coolant channels. Experimental results were determined for the individual outlet coolant channel temperatures under various asymmetric heating conditions. By comparing these results to predicted values assuming no inter-channel mixing, the effect of the rod spacers in changing the coolant channel temperature differences were determined.

Typical asymmetric heating results are shown in Figure 23 for the three rod bundle configurations that have been tested. These results were determined with no power supplied to H-2, in order to create a cross-coolant channel temperature difference from Channels A to B. Channels B receive only two-thirds the test rod heat input that Channels A receive. Under zero crossflow conditions, the predicted cross-coolant channel temperature differences, shown in the first row of Figure 23, were determined by applying the 2/3 factor to the measured axial temperature rise of Channels B obtained under symmetric heating conditions. As is evident from Figure 23, there is considerably greater inter-channel mixing

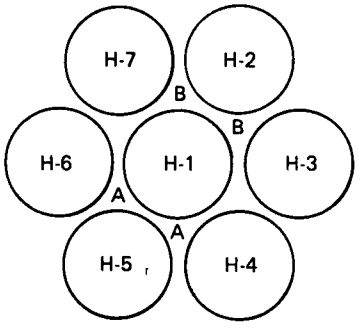

$\Delta T = \overline{T}_A - \overline{T}_B$	CROSS COOLANT ΔT WITH ONE HEATER OFF*		
	SMOOTH TUBES P/D = 1.00	RING SPACERS P/D = 1.05	HELICAL-FIN SPACERS P/D = 1.05
PREDICTED (WITHOUT MIXING)	17	21	16
MEASURED	17	17	9
% REDUCTION	0	19	44

*$\overline{q''_{w_o}}$ = 47,300; Pe = 210

6531-4740

Figure 23. Cross-Coolant Channel Temperature Differences Under Asymmetric Heating Conditions

taking place with the helical-fin configuration, as compared to the ring spacer bundle, both of which have P/D = 1.05. This can be attributed to the fluid tending to follow the helical path of the fins and the R-L-N fin configuration, for which fins on adjacent rods tend to mix the fluid in the same direction. As expected, due to zero spacing between elements, the smooth-tube rod bundle (P/D = 1.00) showed no reduction on the cross-coolant temperature difference.

In addition to the results shown in Figure 23, asymmetric heating tests were performed at other power levels and flow rates. It was found that the conclusions, in terms of percentage changes, were independent of power and flow rate over the range investigated.

VII. CONCLUSIONS AND DISCUSSION OF RESULTS

Three rod bundle configurations were tested under conditions of turbulent longitudinal flow of liquid NaK. Testing was performed in the low-Pe regime (30 to 240), and under the heat flux conditions (28,000 to 110,000 Btu/hr-ft^2) that are considered typical for compact reactor cores. Based upon the experimental results, the following important conclusions can be made:

1) For the tightly packed rod bundle having a P/D = 1.00, excellent agreement was found to exist between the theoretical and experimental results for the cladding circumferential temperature variation and the rod-average heat transfer coefficient.

2) Due to a significant increase in the intra-channel turbulence, negligible circumferential temperature variations were observed for both the ring and helical-fin spacer configurations having a P/D = 1.05.

3) The heat transfer results for the ring spacer configuration showed a slight Pe dependence. For the P/D = 1.00 rod bundle and helical-fin configuration, the cladding azimuthal temperature distributions and the rod-average film coefficient were independent of Pe, over the range investigated.

4) The experimental results confirmed the predicted approximate five-fold increase in the rod-average Nu value for a closely spaced rod arrangement (P/D = 1.05), compared to tightly packed rod arrangement (P/D = 1.00).

5) For the ring spacer configuration, reasonable agreement between the predicted (smooth tubes) and experimental rod-average film coefficient was found. The helical-fin configuration yielded a 53% increase in the rod-average Nu value over the smooth-tube value.

6) The R-L-N helical-fin spacer configuration produced appreciable inter-channel mixing, or crossflow. This was observed for the asymmetric heating tests, in which a 44% reduction in the cross coolant-to-coolant channel temperature difference was found. This reduction was more than twice that observed for the rod bundle employing ring spacers.

The study presented here represents the first time that reliable experimental liquid metal heat transfer data have been obtained for closely spaced rod bundles in the low-Pe regime. The data confirmed earlier expectations that improved heat transfer performance would result from the effect of positive rod spacing and the use of rod spacers. The increased intra-channel turbulence created by the helical-fins negated any rod azimuthal temperature variation, and significantly improved the rod-average film coefficient. The fin-induced inter-channel mixing, or crossflow, was observed to be significant. For an actual ZrH reactor core, the added crossflow will be important in reducing cross fuel element temperature differences, and the resulting bending stresses which occur during asymmetric geometry and heating conditions.

As previously indicated, great care was taken in the experimental loop and test section design, and in insuring a clean liquid metal system. These precautions resulted in obtaining reliable data which can be applied with confidence in the design and analysis of compact reactor cores. It should be noted, however, that the results presented earlier are strictly true only for the conditions of the experimental study. Care must be exercised in applying the present test results to conditions other than those examined.

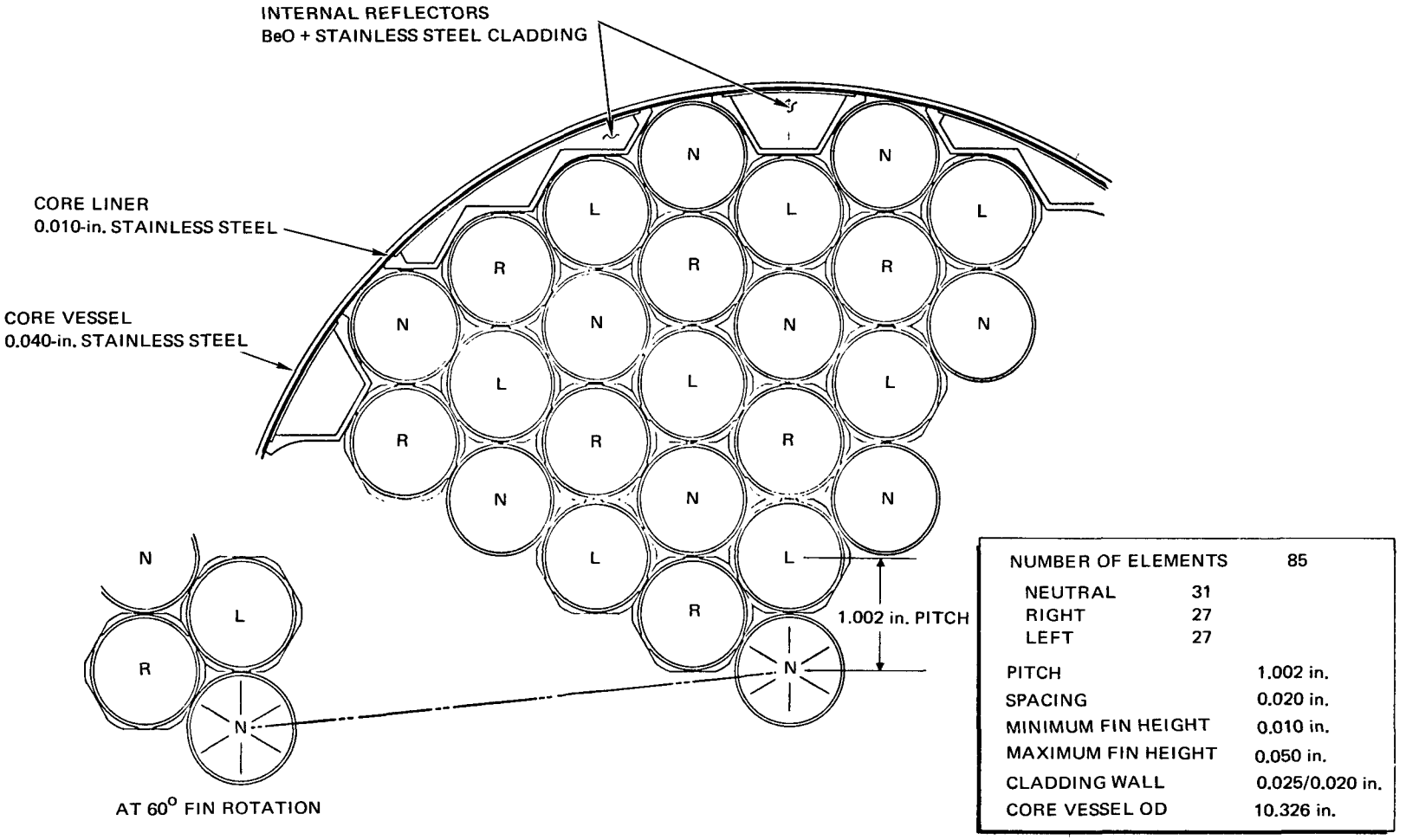

Figure 24. Core Sector

VIII. 5-kwe SYSTEM CORE VERIFICATION TEST

The final heat transfer test would have provided information required for the design and evaluation for the 5-kwe Reactor Thermoelectric System, which would utilize the 1.00-in. hex-shaped, hobbed, finned, fuel rod configuration. Figures 24 and 25 show conceptual designs of the actual core sector and the fuel element configuration. The present status of the above test is described below.

A. HEATER DESCRIPTION

The test rods are special heater assemblies which were designed to simulate ZrH elements, as shown in Figure 26. The test heater assembly consists basically of four (4) cartridge heaters. These cartridge heaters, 4.00 in. in length by 5/8 in. OD, are placed in tandem and wired in parallel to form the heat source. The four cartridge heater subassembly is centered within a smooth or finned cladding tube, and positioned with vibration-packed MgO insulation. Each heater assembly is capable of up to 4 kw of input power, under the test conditions.

B. FINNED ELEMENT DESCRIPTION

The finned elements were machined from Type 304 stainless steel tubing material, 1.125 in. OD with a 0.083 in. wall. The fin width was controlled at 0.125 in., with a minimum fin height of 0.010 in. and a maximum fin height of 0.050 in. The minimum tube wall thickness was 0.020 in. The dimensional features are shown in Figure 27. The method of fabrication of the finned cladding tube is equivalent to that planned for the fuel element cladding for the 5-kwe reactor.

C. CLADDING THERMOCOUPLE DESCRIPTION

Cladding thermocouples are spaced around the inside cladding periphery to measure the rod circumferential temperature distribution. The thermocouples consisted of Chromel-Alumel wires, surrounded by MgO insulation and sheathed in Inconel 600 tubing with an OD of 0.020 in. The cladding tube of each instrumented test rod was drilled at specific azimuthal locations, as shown in Figure 28. The fabricated thermocouples are located azimuthally by means of a special tool, designed for each heater. The thermocouples are inserted $\sim$0.010 in. into the drill holes in the 0.020-in. wall tubing, and TIG welded. This method

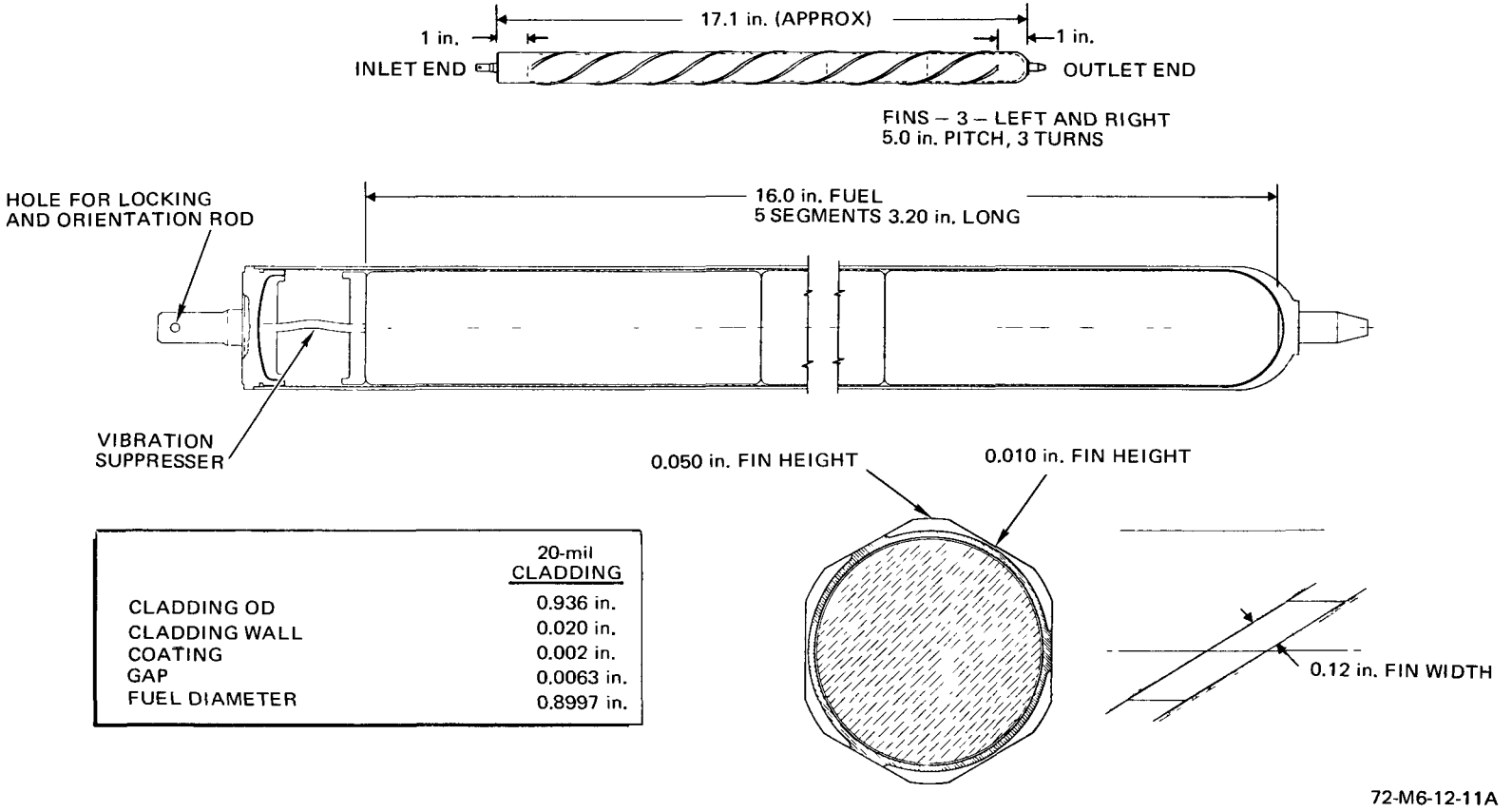

	20-mil CLADDING
CLADDING OD	0.936 in.
CLADDING WALL	0.020 in.
COATING	0.002 in.
GAP	0.0063 in.
FUEL DIAMETER	0.8997 in.

Figure 25. Fuel Element

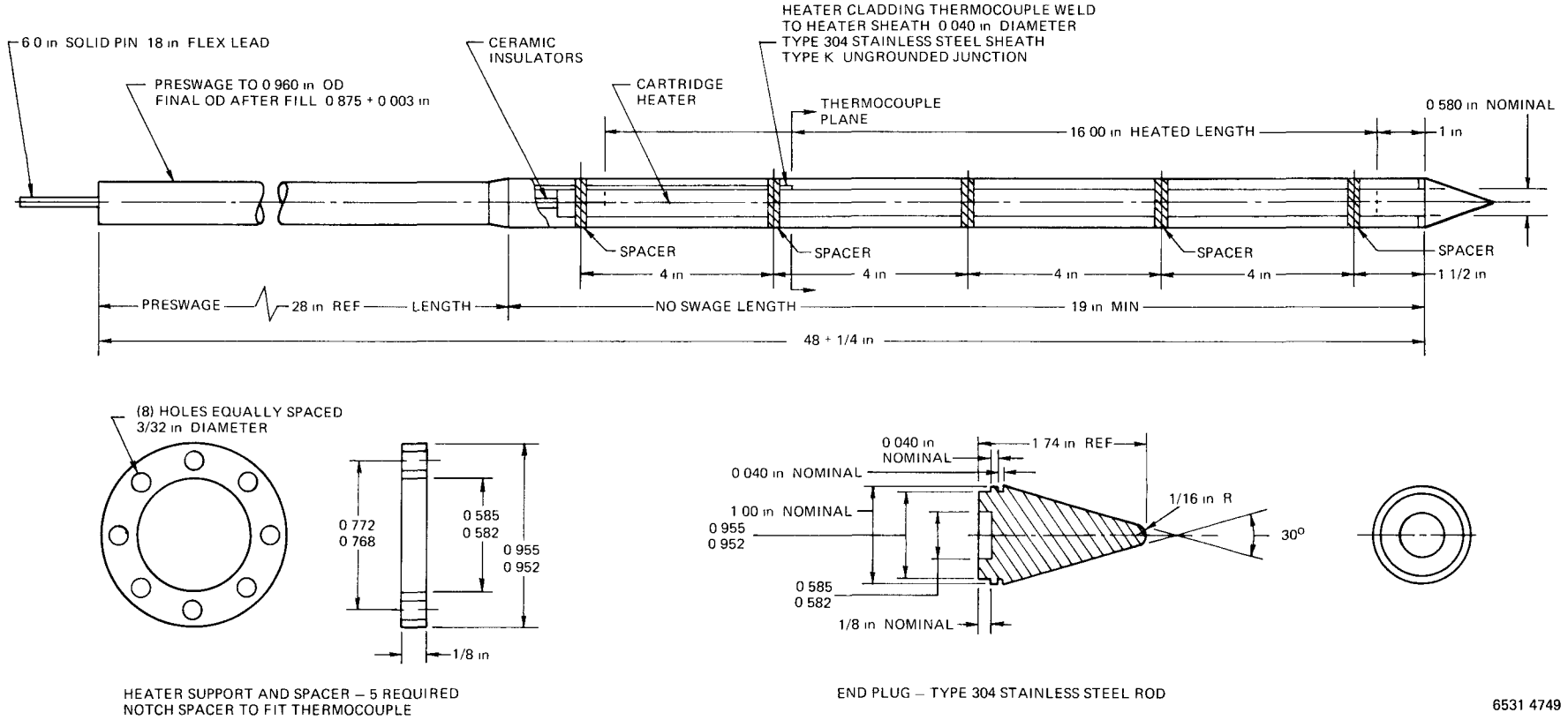

Figure 26. 1.00-in. Heater Element

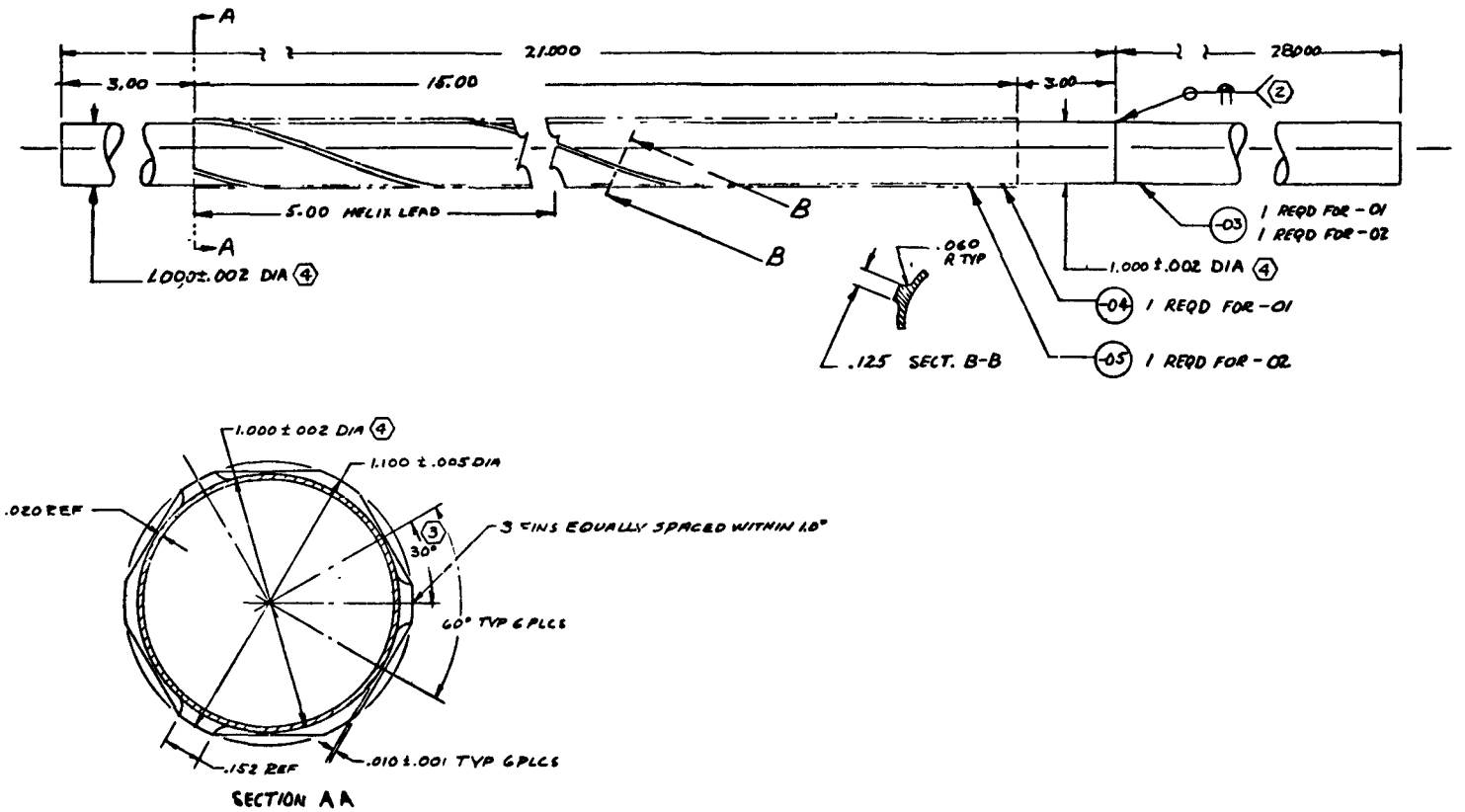

Figure 27. Hobbing of Finned Elements (From Drawing EX-N652200032)

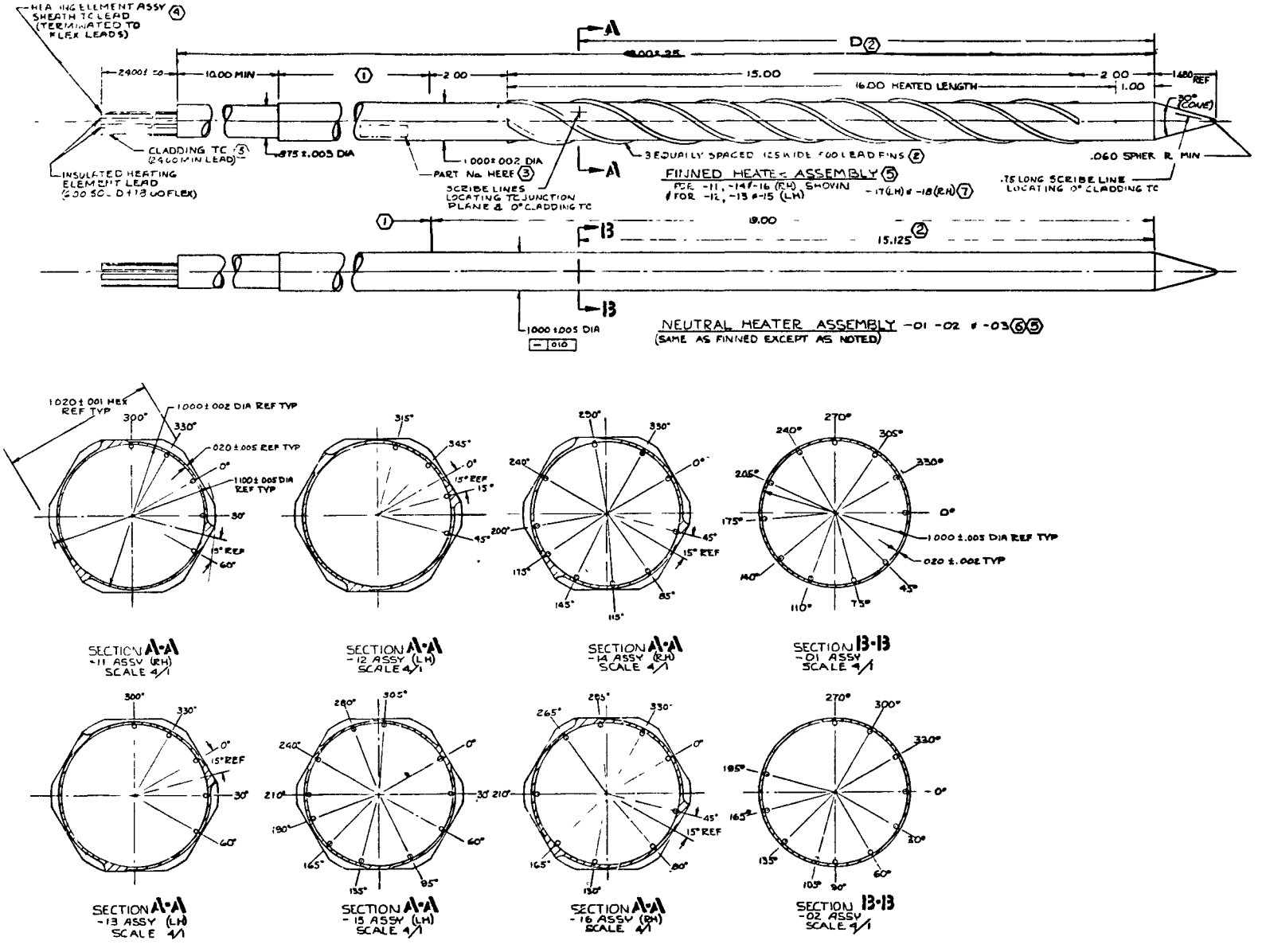

Figure 28. Thermocouple Locations and Installation (From Drawing EX-N652200008)

assures that the thermocouple measurements will be actual wall temperature readings.

D. TEST SECTION DESCRIPTION

The test section consists of 19 electrically heated cylindrical elements, arranged on symmetrical equilateral triangular arrays. The rod bundle configuration corresponds to a P/D ratio of 1.02. The rod bundle is contained within a Type 304 stainless steel cylindrical shell, which has simulated filler pieces attached to the inner wall to maintain a proper coolant flow distribution. The test section is instrumented to measure inlet and outlet coolant temperatures. To achieve a uniform velocity profile at the entrance to the rod bundle, a plenum and bell mouth nozzle arrangement is used at the inlet to the test section.

E CURRENT STATUS OF FINAL CORE VERIFICATION TEST

Due to the ZrH Program fund curtailment, no experimental tests were performed utilizing the previously described test section.

NOMENCLATURE LIST

Symbols

D = rod diameter (ft)

D_h = hydraulic diameter of rod bundle (ft)

g_o gravitational constant (lb_m-ft/lb_f-hr^2)

h = heat transfer coefficient (Btu/hr-ft^2-°F)

k = thermal conductivity (Btu/hr-ft-°F)

L_H heated length (ft)

$Nu = \bar{h}D_h/k_f$ = Nusselt number (dimensionless)

P = pitch, or distance between rod centers (ft)

$Pe = (Re)(Pr)$ = Peclet number (dimensionless)

Pr $\mu C_p/k_f$ Prandtl number (dimensionless)

q = heat flux (Btu/hr-ft^2)

$Re = \rho \bar{u} D_h/\mu$ Reynolds number (dimensionless)

r radial coordinate (ft)

r_3 = inside radius of cladding tube (ft)

R = outside radius of cladding tube (ft)

T = temperature (°F)

W_r heater input power (kw)

z = axial coordinate (ft)

Greek Letters

θ = aximuthal coordinate (radians)

μ viscosity of coolant (lb_m/ft-hr)

ρ = density of coolant (lb_m/ft^3)

Subscripts

b = bulk coolant

F flow development, fuel or MgO region of test rod

f = coolant

H = heated region of test rod, thermal profile development

i inside, local

o outside

S spacer rings

w = cladding wall

Other

ΔT_{CORR} cladding thermocouple correction factor

ΔT_f average film temperature drop

NA = not applicable

P/D = pitch-to-diameter ratio

R-L-N = right-left-neutral configuration

T/C thermocouple

$T_{w_i}(\theta) - T_b$ differential between cladding inner wall temperature and bulk coolant temperature

z_F/D_h cladding thermocouple location with respect to velocity profile development

z_H/D_h cladding thermocouple location with respect to temperature profile development

z_H/L_H = cladding thermocouple location with respect to heated length

z_S/D_h = cladding thermocouple location with respect to middle spacer rings

$\overline{(\ )}$ $\frac{6}{\pi}\int_o^{\pi/6} (\ )d\theta$ average value

BLANK

REFERENCES

1. A. R. Marchese, "Analytical Study of Heat Transfer to Liquid Metals Flowing Parallel Through Tightly Packed Fuel Rod Bundle," Liquid Metal Heat Transfer and Fluid Dynamics Symposium, ASME Winter Annual Meeting, New York City (November 1970) p 15

2. A. R. Marchese, "Experimental Study of Heat Transfer to NaK Flowing In-Line Through a Tightly Packed Rod Bundle," AIChE-ASME 13th National Heat Transfer Conference, Denver, Colo., AIChE Paper No. 36 (August 1972)

3. A. R. Marchese, "Influence of Rod Spacers on the Heat Transfer to a Liquid Metal Flowing In-Line Through a Closely Spaced Rod Bundle," (to be presented at Liquid Metal Heat Transfer in Nuclear Plant Components Symposium, 14th National ASME-AIChE Heat Transfer Conference, Atlanta, Georgia, (August 5-8, 1973)

4. O. E. Dwyer et al., "Heat Transfer to Mercury Flowing In-Line Through an Unbaffled Rod Bundle: Experimental Study of the Effect of Rod Displacement on Rod-Average Heat Transfer Coefficients," Trans. ASME, Ser. C., J. Heat Trans., 91 (1969) p 568

5. O. E. Dwyer et al., "Heat Transfer to Mercury Flowing In-Line Through an Unbaffled Rod Bundle: Effect of Rod Displacement on Local Surface Temperature and Local Heat Flux," Proceedings of the Fourth International Heat Transfer Conference, Paris (1970)

6. C. J. Hsu, "Effect of Rod Displacement on Heat Transfer in Slug Flow Through Unbaffled Rod Bundles," Liquid Metal Heat Transfer and Fluid Dynamics Symposium, ASME Winter Annual Meeting, New York City (November 1970) p 58

7. C. J. Hsu, "Multiregion Analysis of the Effect of Rod Displacement on Heat Transfer in Slug Flow Through Closely Packed Rod Bundles," Nucl. Sci. Eng., 47, 3 (1970) p 380

8. V. I. Subbotin et al., "Heat Removal from Reactor Fuel Elements Cooled by Liquid Metals," Paper No. 328, Third United Nations International Conference on the Peaceful Uses of Atomic Energy, Geneva (August 31-September 9, 1964)

9. V. I., Subbotin et al., "Heat Exchange During the Flow of Mercury and Water in a Tightly Packed Rod Pile," J. of Soviet Atomic Energy (1960), translated from Atomnaya Energiya, 9, No. 6 (1960) pp 461-469

10. O. E. Dwyer, "Recent Developments in Liquid Metal Heat Transfer," Atomic Energy Review, 4, No. 1 (1966) pp 3-92

11. Y. D. Levchenko et al. "The Distribution of Coolant Velocities and Wall Stresses in Closely Packed Rods," J. of Soviet Atomic Energy (1967), translated from Atomnaya Energiya, 22, No. 3 (1966) p 218

12. W. Eifler and R. Nijsing, "Experimental Investigation of Velocity Distribution and Flow Resistance in a Triangular Array of Parallel Rods," Nucl. Eng. Design, 5 (1967) p 22

13. Sodium and NaK Supplement – Liquid Metals Handbook, U. S. Atomic Energy Commission (1970 ed.)

14. A. V. Zhukov et al., "Heat Transfer from Loosely-Spaced Fuel Rod Clusters to a Liquid Metal Flowing in the Axial Direction," NASA Technical Translation, Liquid Metals, NASA TT F-522 (1969) p 149